frontiers | Frontiers in Plant Science

TYPE Original Research
PUBLISHED 13 June 2024
DOI 10.3389/fpls.2024.1388537

OPEN ACCESS

EDITED BY
Stefan Wanke,
Goethe University Frankfurt, Germany

REVIEWED BY
Craig Barrett,
West Virginia University, United States
Isabel Marques,
Universidade de Lisboa, Portugal

*CORRESPONDENCE
Stephanie Goedderz
stephanie.goedderz@jcu.edu.au
Katharina Nargar
katharina.nargar@csiro.au

RECEIVED 20 February 2024
ACCEPTED 13 May 2024
PUBLISHED 13 June 2024

CITATION
Goedderz S, Clements MA, Bent SJ, Nicholls JA, Patel VS, Crayn DM, Schlüter PM and Nargar K (2024) Plastid phylogenomics reveals evolutionary relationships in the mycoheterotrophic orchid genus *Dipodium* and provides insights into plastid gene degeneration.
Front. Plant Sci. 15:1388537.
doi: 10.3389/fpls.2024.1388537

Plastid phylogenomics reveals evolutionary relationships in the mycoheterotrophic orchid genus *Dipodium* and provides insights into plastid gene degeneration

Stephanie Goedderz[1,2]*, Mark A. Clements[3], Stephen J. Bent[4], James A. Nicholls[5], Vidushi S. Patel[6], Darren M. Crayn[1], Philipp M. Schlüter[2] and Katharina Nargar[1,6]*

[1]Australian Tropical Herbarium, James Cook University, Cairns, QLD, Australia, [2]Department of Plant Evolutionary Biology, Institute of Biology, University of Hohenheim, Stuttgart, Germany, [3]Centre for Australian National Biodiversity Research (joint venture between Parks Australia and CSIRO), Canberra, ACT, Australia, [4]Data61, Commonwealth Industrial and Scientific Research Organisation (CSIRO), Brisbane, QLD, Australia, [5]Australian National Insect Collection, Commonwealth Industrial and Scientific Research Organisation (CSIRO), Canberra, ACT, Australia, [6]National Research Collections Australia, Commonwealth Industrial and Scientific Research Organisation (CSIRO), Canberra, ACT, Australia

The orchid genus *Dipodium* R.Br. (Epidendroideae) comprises leafy autotrophic and leafless mycoheterotrophic species, with the latter confined to sect. *Dipodium*. This study examined plastome degeneration in *Dipodium* in a phylogenomic and temporal context. Whole plastomes were reconstructed and annotated for 24 *Dipodium* samples representing 14 species and two putatively new species, encompassing over 80% of species diversity in sect. *Dipodium*. Phylogenomic analysis based on 68 plastid loci including a broad outgroup sampling across Orchidaceae found that sect. *Leopardanthus* is the sister lineage to sect. *Dipodium*. *Dipodium ensifolium*, the only leafy autotrophic species in sect. *Dipodium*, was found to be a sister to all leafless, mycoheterotrophic species, supporting a single evolutionary origin of mycoheterotrophy in the genus. Divergence-time estimations found that *Dipodium* arose ca. 33.3 Ma near the lower boundary of the Oligocene and that crown diversification commenced in the late Miocene, ca. 11.3 Ma. Mycoheterotrophy in the genus was estimated to have evolved in the late Miocene, ca. 7.3 Ma, in sect. *Dipodium*. The comparative assessment of plastome structure and gene degradation in *Dipodium* revealed that plastid *ndh* genes were pseudogenised or physically lost in all *Dipodium* species, including in leafy autotrophic species of both *Dipodium* sections. Levels of plastid *ndh* gene degradation were found to vary among species as well as within species, providing evidence of relaxed selection for retention of the NADH dehydrogenase complex within the genus. *Dipodium* exhibits an early stage of plastid genome degradation, as all species were found to have retained a full set

of functional photosynthesis-related genes and housekeeping genes. This study provides important insights into plastid genome degradation along the transition from autotrophy to mycoheterotrophy in a phylogenomic and temporal context.

KEYWORDS

Dipodium, divergence-time estimation, gene degradation, mycoheterotrophy, phylogenetics, plastome

1 Introduction

Heterotrophic plants—plants that rely on other organisms for energy and nutrients—are remarkable survivors, exhibiting often curious morphological, physical, or genomic modifications, reflecting evolutionary relaxed selective pressure on photosynthetic function (Graham et al., 2017; Barrett et al., 2019). Advances in next-generation sequencing and bioinformatic pipelines have vastly accelerated the characterisation of plastid genomes (plastomes), including heterotrophic plants, providing new insights into plastome evolution. Plastomes of heterotrophic plants often exhibit greatly altered structure and gene content due to photosynthesis-related genes that are no longer required (Delannoy et al., 2011; Barrett et al., 2014; Lam et al., 2015; Braukmann et al., 2017; Graham et al., 2017; Barrett et al., 2018; Wicke and Naumann, 2018; Barrett et al., 2019; Qu et al., 2019; Klimpert et al., 2022; Peng et al., 2022; Wen et al., 2022). Hence, heterotrophic plants offer excellent opportunities to gain insight into plastome evolution under relaxed selection.

Early non-phylogenomic studies on plastome evolution in heterotrophic plants allowed the discovery of large-scale plastome evolutionary patterns and stimulated research into fine-scale, phylogenetic comparative approaches (e.g., Delannoy et al., 2011; Logacheva et al., 2011; Roma et al., 2018). Thus far, most phylogenetic comparative studies included plastomes of taxa scattered across families, tribes, or genera (e.g., Kim et al., 2015; Feng et al., 2016; Niu et al., 2017; Lallemand et al., 2019; Kim et al., 2020; Li et al., 2020; Tu et al., 2021; Kim et al., 2023). Nevertheless, phylogenetic, comparative approaches at the infrageneric level are still scarce (e.g., Barrett et al., 2018, 2019).

Orchidaceae, one of the two largest flowering plant families, has undergone a greater number of independent transitions from autotrophy to heterotrophy than any other land plant lineage (Merckx, 2013; Christenhusz and Byng, 2016; Jacquemyn and Merckx, 2019). The family comprises several heterotrophic orchid lineages that rely to some extent on mycorrhizal fungi for carbon and other nutrients, i.e., initial, partial, or full mycoheterotrophy (Merckx, 2013).

So far, most examined mycoheterotrophic orchid plastomes exhibited degradation patterns similar to those found in heterotrophic plastomes of other plants. These include a reduction in genome size, a decrease in guanine–cytosine (GC) content, rearrangements, pseudogenisations, and gene losses (e.g., Delannoy et al., 2011; Barrett et al., 2018, 2019; Lallemand et al., 2019; Wen et al., 2022). Moreover, whole plastome sequencing has revealed patterns of plastid gene degradation for various heterotrophic plastomes that led to the development of conceptual models to predict the evolutionary transition from autotrophy to heterotrophy of the plastid organelle (e.g., Graham et al., 2017; Barrett et al., 2019). Several studies in mycoheterotrophic orchid lineages found support for these models that predict a progression from losses of the chloroplast *ndh* genes to genes encoding complexes that are directly involved in photosynthesis (e.g., *psa* and *psb*) to more general "housekeeping" genes (e.g., *acc*D and *mat*K) (Barrett et al., 2018; Wicke and Naumann, 2018; Barrett et al., 2019; Kim et al., 2020, 2023).

Interestingly, degraded *ndh* genes were also found in some autotrophic orchids (e.g., Kim et al., 2015; Kim and Chase, 2017; Niu et al., 2017; Lallemand et al., 2019; Kim et al., 2023). This appears curious, as the *ndh* genes encode proteins of the NADH dehydrogenase complex (NDH complex), which is assumed to play a role in cyclic electron flow and thus fine-tunes photosynthesis (Yamori et al., 2015; Peltier et al., 2016). The degradation of *ndh* genes is hypothesised to have led to additional structural changes in the plastome (Kim et al., 2015). In particular, *ndh*F gene loss was correlated with shifts in the position of the junction of the inverted repeat/small single copy (IR/SSC) region in Orchidaceae and other plants (Kim et al., 2015; Niu et al., 2017; Dong et al., 2018; Roma et al., 2018; Thode and Lohmann, 2019; Könyves et al., 2021; Li et al., 2021). However, within Orchidaceae, degradation of *ndh* genes was found to vary even among closely related species (e.g., Kim et al., 2015; Feng et al., 2016; Kim and Chase, 2017; Barrett et al., 2018, 2019), which suggests the genes for the NDH complex may be under relaxed selective pressure in several orchid lineages (Kim and Chase, 2017). Moreover, previous studies found that *ndh* degradation patterns vary considerably and have been independently degraded among orchids (Kim et al., 2015; Kim and Chase, 2017; Niu et al., 2017; Lallemand et al., 2019).

The orchid genus *Dipodium* R.Br. (Cymbidieae) contains both autotrophic and mycoheterotrophic species and thus represents a suitable model system in which to address hypotheses of plastome evolution. The genus comprises 39 species and is divided into two sections, *Dipodium* and *Leopardanthus* (Blume) O. Kuntze, based on morphological and geographical evidence (O'Byrne, 2017; Jones, 2021). Sect. *Leopardanthus* (26 species) is distributed in the floristic regions of Malesia and Australasia (O'Byrne, 2017). All species of

sect. *Leopardanthus* are green leafy plants and non-uniform in habit (O'Byrne, 2017). Section *Dipodium* (13 species) occurs predominantly in Australasia, with nearly all species being endemic to Australia. One species occurs in New Guinea (*Dipodium elatum* J.J. Sm.), one species extends into the Pacific region [*Dipodium squamatum* (G.Forst.) Sm. (New Caledonia and Vanuatu)], and one occurs in Malesia (*Dipodium gracile* Schltr. (Sulawesi) (Schlechter, 1911; O'Byrne, 2017; POWO, 2023; WFO, 2023). In contrast to sect. *Leopardanthus*, most species of sect. *Dipodium* are non-climbing terrestrials, forming subterranean rhizomes and erect flowering stems with highly reduced, non-photosynthetic leaves (i.e., scales) (Figure 1B). Leafless species within sect. *Dipodium* are generally assumed to be mycoheterotrophic (O'Byrne, 2014). However, the extent to which non-leafy species in *Dipodium* are mycoheterotrophic is unclear. Whereas they have been assumed to be fully heterotrophic in the past, recent research in *Dipodium roseum* points to partial instead of full mycoheterotrophism (McLay et al., 2023). Among the Australian species of sect. *Dipodium*, *Dipodium ensifolium* F. Muell. stands out as a leafy terrestrial (Figure 1A).

The aims of this study were as follows:

1. sequence and assemble plastid genomes for species of *Dipodium* to elucidate patterns of plastid genome modification (e.g., rearrangement, structural variation, pseudogenisation, and gene loss) across autotrophs and mycoheterotrophs within the genus and examine gene degradation in the context of current models of plastome degradation in heterotrophic plants,

FIGURE 1
Habit and flowers of *Dipodium* sect. *Dipodium*. **(A)** *Dipodium ensifolium*. **(B)** *D. elegantulum* (note the green to purplish inflorescence stem). **(C)** *D. ensifolium*. **(D)** *D. interaneum*. **(E)** *D. elegantulum*. **(F)** *D. variegatum*. **(G)** *D. punctatum*. **(H)** *D. roseum*. Photos: **(A–C, E)** S. Goedderz; **(D, F–H)** M.A. Clements.

2. infer phylogenomic relationships within section *Dipodium* and among closely related autotrophic relatives (i.e., *Dipodium* section *Leopardanthus*), and
3. estimate divergence times of *Dipodium* to assess the origin of mycoheterotrophy within the genus and elucidate over which evolutionary timeframe plastid gene degradation and losses have taken place within *Dipodium*.

2 Material and methods

2.1 Plant material

For this study, we sampled all known Australian species of section *Dipodium* and one representative of section *Leopardanthus* (Table 1). Based on previous molecular systematic studies (Serna-Sánchez et al., 2021; Pérez-Escobar et al., 2023; Zhang et al., 2023), an extended outgroup from closely related orchid genera within subtribe Eulophiinae (*Eulophia* R.Br., *Geodorum* Andrews) and subtribe Cymbidiinae (*Cymbidium* Sw., *Acriopsis* Reinw. ex. Blume) was sampled (Table 1). Specimens studied were from different regions within Australia, with the exception of one specimen from Papua New Guinea (*Dipodium pandanum 2*) (Table 1).

2.2 DNA extraction, library preparation, and sequencing

Standard plant DNA extractions were carried out from 5–20 mg of silica-dried plant tissue from field collections or herbarium material (Table 1) at the National Research Collections Australia (NRCA; CSIRO) in Canberra. The Invisorb DNA Plant HTS96 kit

TABLE 1 Plant material used in this study includes voucher details and provenances with botanical districts.

Species	DNA extract no.	Voucher details	Provenance
Dipodium aff. *roseum* 1	HTCG 0828	C. Bower ORG7817 (CANB 906470.1)	AU: NSW; Central Tablelands; Mullions Range State Forest
Dipodium aff. *roseum* 2	HTCG 0830	C. Bower ORG7818 WP 6 (CANB 906471.1)	AU: NSW; Central Tablelands; Mount Canobolas State Conservation Area
Dipodium aff. *roseum* 3	HTCG 0831	C. Bower ORG7818 WP 7 (CANB 906471.1)	AU: NSW; Central Tablelands; Mount Canobolas State Conservation Area
Dipodium aff. *roseum* 4	HTCG 0832	C. Bower ORG7818 WP 9,10,11 (CANB 906471.1)	AU: NSW; Central Tablelands; Mount Canobolas State Conservation Area
Dipodium aff. *stenocheilum*	HTCG 1691	D.L. Jones 8968 (CBG 9220253.1)	AU: QLD; Cook; Mount Elliot
Dipodium ammolithum	HTCG 1372	M.D. Barrett 4910A (PERTH)	AU: WA; North Kimberley, Theda Station
Dipodium atropurpureum 1	HTCG 0760	W.M. Dowling DC 1717 (CANB 924629.1)	AU: NSW; Northern Tablelands; Barrington Tops State Forest
Dipodium atropurpureum 2	HTCG 1679	M.A. Clements 4426 (CBG 8605570.1)	AU: NSW; Northern Tablelands; New England Highway to Armidale
Dipodium basalticum	HTCG 1693	D.E. Murfet 4837 (CANB 662327.1)	AU: NT; Darwin and Gulf; near Nhulunbuy
Dipodium campanulatum 1	HTCG 1680	K. Alcock DLJ5622 (CBG 9004646.2)	AU: SA; South-east; Naracoorte
Dipodium campanulatum 2	HTCG 1681	D.E. Murfet 1930b (CANB 677107.2)	AU: SA; South-east; Penola Conservation Park
Dipodium elegantulum	HTCG 1682	L. Lawler 8 (CBG 8605836.1)	AU: QLD; Cook; near Mareeba
Dipodium ensifolium	HTCG 1343	D.M. Crayn 1581 (CNS 145658.1)	AU: QLD; Cook; record is Queensland sensitive
Dipodium hamiltonianum	HTCG 1683	D.L. Jones & P.D. Jones s.n. (CANB)	AU: QLD; Moreton; Currimundi
Dipodium interaneum	HTCG 0181	J. Egan ORG7745 (CANB)	AU: ACT; Canberra; Birrigai
Dipodium pandanum 1	CNS_G01262	B. Gray 8233 (CANB 572368.2)	AU: QLD; Kennedy North; near Coen; record is Queensland sensitive
Dipodium pandanum 2	HTCG 1694	M. Jacobs 8984 (CANB 576763.1)	PG: Mount Bosavi
Dipodium pardalinum 1	HTCG 1684	D.L. Jones 12834 (CBG 9603749.1)	AU: VIC; Victorian Volcanic Plain; Heathmere
Dipodium pardalinum 2	HTCG 1685	D.L. Jones 12830 (CBG 9603745.1)	AU: VIC; Victorian Volcanic Plain; Heathmere
Dipodium pulchellum	HTCG 1686	D.L. Jones s.n. (CANB)	AU: QLD; Moreton; Green Mountains
Dipodium punctatum	HTCG 0827	C. Bower ORG7816 (CANB 906469.1)	AU: NSW; Central Tablelands; Black Salee Reserve
Dipodium roseum 1	HTCG 1687	C. Houston ORG3859 (CANB 656733.1)	AU: SA; Lofty South; Wotton Scrub

(Continued)

TABLE 1 Continued

Species	DNA extract no.	Voucher details	Provenance
Dipodium roseum 2	HTCG 1688	C. Houston ORG3859 (CANB 656733.2)	AU: SA; Lofty South; Wotton Scrub
Dipodium stenocheilum 1	HTCG 1689	M.A. Clements 1189 (CBG 7801007.1)	AU: NT; Darwin and Gulf; Elcho Island
Dipodium stenocheilum 2	HTCG 1690	D.E. Murfet 3018 (CANB 619696.1)	AU: NT; Darwin and Gulf; Livingston
Dipodium variegatum	HTCG 1692	D.L. Jones 1280 (CANB 665182.1)	AU: QLD; Moreton; Beenleigh
Outgroup			
Acriopsis emarginata	CNS_G00305	C.D. Kilgour 634A (CNS 135324.1)	AU: QLD, Cook, Daintree National Park
Cymbidium canaliculatum	CNS_G00165	K.R. McDonald, 11722 (BRI AQ0831415)	AU: QLD, Cook, Mungkan Kandju National Park
Eulophia bicallosa	HTCG 1696	I. Morris (DLJ 4579) (CBG 8913381.1)	AU: NT; Darwin and Gulf; Howard Springs
Eulophia graminea	CNS_G02766	C.P. Brock 311 (CANB 596921.1)	AU: NT; Darwin
Eulophia nuda	HTCG 1697	R. Crane 1072 (CANB)	cult. ex AU: QLD; Moreton; Caloundra
Geodorum densiflorum	CNS_G01890	K. Schulte 254B (CNS 146066.1)	AU: QLD; Cairns region
Oeceoclades pelorica	HTCG 1695	J. Taylor s.n. (CBG 7905124.1)	cult. ex AU: QLD; Cook; Iron Range

Taxonomy according to the Australian Plant Census (APC, 2023). CANB, Australian National Herbarium; CNS, Australian Tropical Herbarium; AU, Australia; PG, Papua New Guinea; ACT, Australian Capital Territory; NT, Northern Territory; NSW, New South Wales; SA, South Australia; QLD, Queensland; WA, Western Australia; VIC, Victoria.

(Stratec, Birkenfeld, Germany) was used following the manufacturer's protocol, with a final elution of 60 µL.

DNA of *Dipodium* samples (Table 1) was sonicated to an average target length of ca. 200 base pairs (bp) using a LE220 sonicator (Covaris, Bankstown, Australia). After sonication, DNA length and concentration were quantified on Fragment Analyzer (Agilent Technologies, Santa Clara, CA, USA) using the Agilent high-sensitivity genomic DNA kit.

DNA libraries were prepared using the QiaSeq UltraLow Input library kit (Qiagen, Germantown, Australia) using custom dual-indexed adapters. Final libraries were size-selected on Fragment Analyzer using the high-sensitivity Genomic Fragment Analyzer Kit (Agilent, Santa Clara, CA, USA), quantified using the Fluoroskan plate fluorometer (Thermo Fisher, Waltham, MA, USA) and the Quant-iT HS dsDNA kit (Invitrogen, Carlsbad, CA, USA) following the manufacturer's instructions. Samples were pooled equimolarly and sequenced using 150 bp paired-end reads on a NovaSeq S1 flowcell (Illumina, San Diego, CA, USA) at the Biomolecular Resource Facility within the John Curtin School of Medical Research, Australian National University (Canberra, Australia). For some samples (prefixed CNS), DNA libraries were prepared using the TruSeq Nano DNA LT library preparation kit (Illumina, San Diego, CA, USA) with an insert size of 350 bp, following the manufacturer's protocols. Pooled libraries (96x) were sequenced on an Illumina HiSeq 2500 platform with 125 bp paired-ends at the Australian Genomic Research Facility, Melbourne (Australia).

2.3 Data processing and whole plastid genome assembly

Both *de novo* and reference-guided assemblies were carried out for the *Dipodium* dataset. Trimming and assembly of *de novo* contigs were carried out as described by Nargar et al. (2022). Briefly, raw sequences were trimmed by applying a Phred score >20 using Trimmomatic 0.39 (Bolger et al., 2014) and deduplicated using "clumpify" from BBtools 38.9 (Bushnell, 2014). Read pairs were *de novo* assembled using SPAdes 3.15 (Bankevich et al., 2012) and GetOrganelle (v1.7.7.0) (Jin et al., 2020) using default settings. Plastid databases were extracted from the National Center for Biotechnology Information (NCBI) Nucleotide Entrez database using Entrez Programming Utilities (2008) using taxonomic, keyword, and sequence length constraints. Contigs were identified as derived from plastid source using blastn against these databases. Genes within plastid contigs were identified by homology using BLAST (Altschul et al., 1990) and BLASTx (RRID: SCR_001653) against genes extracted from annotations of the reference sequence sets extracted from nuccore.

Reference-guided assemblies were performed with paired, merged reads and the recently published and closely related plastome of *D. roseum* D.L. Jones and M.A. Clem. (MN200386, Kim et al., 2020). The related orchid *Masdevallia coccinea* Linden ex Lindl. (KP205432, Kim et al., 2015) was included as an additional reference sequence to ensure that regions that already showed degradation in some plastid genes in the plastome of *D. roseum* (e.g., all *ndh* genes) (MN200386, Kim et al., 2020) and which may still be present in other *Dipodium* species could be assembled, as the plastome of *M. coccinea* has a full set of functional plastid genes (Kim et al., 2015).

Reference-guided assemblies were carried out using the plugin "map to reference" in Geneious Prime (Version 2022.0.2, Biomatters Ltd., www.geneious.com) with default settings. To obtain complete plastome assemblies, consensus sequences for each sample were extracted (threshold 60%, reading depth >10), aligned using MAFFT v7.388 (Katoh and Standley, 2013) in Geneious, manually checked, and compared. Reference-guided assemblies were visually inspected and compared to *de novo* assemblies obtained with SPAdes and

GetOrganelle based on alignments generated with MAFFT v7. 388 in Geneious. In cases of misassembled regions due to potential mismatches between the sample and the reference plastome in reference-guided assemblies, *de novo* assemblies were consulted and the region extracted from the *de novo* assembly were quality allowed. The prediction and finding of gene annotations for complete plastome assemblies were performed using the Geneious plugin "predict annotation" [similarity, 90%; best match with *D. roseum* (MN200386)]. Open reading frames (ORFs) were manually checked and verified by identifying the start and stop codons. In cases of remaining ambiguities, BLAST searches were conducted for reading-frame verification (Altschul et al., 1990). The IR boundaries were identified using the "repeat finder" plugin in Geneious with default settings.

In total, 24 complete *Dipodium* plastomes were assembled in this study and are available in the CSIRO Data Access Portal (DOI: https://doi.org/10.25919/6wcx-0h88). The graphical representation of each plastome and divergent regions with annotations was created using OrganellarGenomeDRAW (OGDRAW, version 1.3.1, Greiner et al., 2019).

2.4 Phylogenetic analyses

To elucidate phylogenetic relationships within *Dipodium* and to assess the phylogenetic position of *Dipodium* within Cymbidieae, we performed a phylogenetic analysis with DNA sequences of 33 newly sequenced plastomes from this study (Table 1) and an extended outgroup sampling for 115 samples from published plastid data (Supplementary Material 1).

Coding regions of the respective genes of 33 samples were extracted using the "extract" function in Geneious Prime. Where mutations had led to frameshifts with internal stop codons, the affected sequences were excluded from phylogenetic analyses.

Each extracted coding region of a total of 68 plastid loci from 33 samples (including the intron regions) and 115 published plastomes (excluding intron regions) were aligned using MAFFT Geneious prime plugin (v7.388; Katoh et al., 2002; Katoh and Standley, 2013) with default settings, checked manually, and subsequently concatenated to an alignment of 69,335 bp (Supplementary Material 2).

Maximum likelihood analysis of the plastid dataset (148 samples) with best-fit models GTR+I+I+F+R4 and partitioning schemes of ModelFinder was performed using IQ-TREE ver. 2.2.0 (Nguyen et al., 2015; Kalyaanamoorthy et al., 2017; Minh et al., 2020). Branch support was obtained with the Shimodaira-Hasegawa-like approximate Likelihood Ratio Test (SH-aLRT; Guindon et al., 2010) and the ultrafast bootstrap (ufboot2; Hoang et al., 2018) as implemented in the IQ-TREE software. The tree topology was visualised using the software Figtree (ver. 1.4.4.; http://tree.bio.ed.ac.uk/software/figtree/).

2.5 Divergence-time analysis

For divergence-time estimations of *Dipodium*, the alignments were reduced to the 30 most parsimony-informative loci due to computational limitations. The 30 plastid loci were selected based on their most parsimony-informative (Pi) sites estimated using MEGA (Molecular Evolutionary Genetics Analysis; ver. 11.0.11, Tamura et al., 2021) and the presence of loci across the dataset (Supplementary Material 2). For taxa represented by more than one sample, duplicates were removed from alignments as recommended for divergence-time estimation. Alignments of 30 plastid loci from 134 taxa were concatenated, yielding a total alignment length of 27,934 bp using MAFFT (v7.388; Katoh et al., 2002; Katoh and Standley, 2013) implemented in Geneious Prime (Supplementary Material 2). Absolute node ages and phylogenetic relationships were jointly estimated in BEAST (ver. 2.7.4; Bouckaert et al., 2014, 2019), applying the best-fit model as determined by IQ-TREE's ModelFinder (GTR+F+I+I+R4). Four different models were tested: a Bayesian optimised relaxed and a strict molecular clock with uncorrelated lognormal rates with each a Yule and a birth–death tree prior to the speciation process (Yule, 1925; Zuckerkandl and Pauling, 1965; Gernhard, 2008; Douglas et al., 2021). Trees were calibrated with four secondary calibration points based on Zhang et al. (2023). A normal distribution with an offset value of 101.52 Ma and a standard deviation (SD) of 2.2 was assigned as the crown age of Orchidaceae. The priors for the three other calibration points were set with a normal distribution and the means of stem ages for Vanilloideae (offset value = 93.48 Ma, SD = 2.7), Cypripedioideae (offset value = 89.14 Ma, SD = 2.71), and Orchidoideae (offset value = 77.74 Ma, SD = 2.0). For each clock model, 10 parallel BEAST analyses with each 30 million generations and a sampling frequency of every 10,000 generations were carried out. The run parameters were examined in TRACER (ver. 1.7.2; Rambaut et al., 2018), and the effective sample sizes (ESSs) of >200 for all parameters and the burn-in were assessed. The runs were combined in LogCombiner (Drummond and Rambaut, 2007) with a burn-in of 10% and subsequently used to generate a maximum-clade-credibility chronogram with mean node heights in TreeAnnotator (Drummond and Rambaut, 2007). To determine the best fitting clock model and speciation models for the dataset, a model comparison using the Akaike information criterion by Markov chain Monte Carlo (MCMC) (AICM) was performed using BEAST v.2.6.2 and evaluated using the AIC model selection criterion of Fabozzi et al. (2014).

2.6 Plastid genome evolution

2.6.1 Structural variation in *Dipodium* plastomes

To examine structural variation among the plastomes of *Dipodium*, whole plastome alignments were generated using MAFFT (v7.388; Katoh et al., 2002; Katoh and Standley, 2013) implemented in Geneious Prime with full annotations. Alignments were manually checked, in cases of divergent regions, e.g., the operon region of *ndh*C, *ndh*K, and *ndh*J genes or junctions between the large single copy (LSC)/inverted repeat B (IRB)/SSC/inverted repeat A (IRA) regions; respective regions (including annotations) were extracted in Geneious Prime, separately aligned, proofread, and subsequently visualised using OGDRAW (ver. 1.3.1, Greiner et al., 2019).

10.3389/fpls.2024.1388537

2.6.2 Functional genes, pseudogenes, and physical gene loss

To classify the level of degradation of plastid genes in *Dipodium*, we used the following categories. 1) *Functional*: The reading frame was intact, and less than 10% of the open reading frame was disrupted by small indels. 2) *Moderately pseudogenised*: Less than 10% of the open reading frame was disrupted by internal stop codons or indels, causing non-triplet frameshifts. 3) *Severely pseudogenised*: More than 10% of the open reading frame was disrupted by internal stop codons, large deletions (>10%), or non-triplet frameshifts (based on Barrett et al., 2019). 4) *Lost*: The gene was not identified in the annotation process of the *de novo* assembly (e.g., Joyce et al., 2018) and/or was not detectable within the reference-guided assembly. A gene was considered as not detectable within the reference-guided mapping process if at least 70% of the gene sequence could not be identified for calculation of the consensus sequence within the Geneious mapping process. The coded matrix of gene degradation was plotted against the maximum likelihood phylogenetic tree of *Dipodium*.

3 Results

3.1 Phylogenetic placement of *Dipodium* in tribe Cymbidieae and infrageneric relationships within the genus

The maximum likelihood analysis based on 68 plastid loci and 148 samples yielded highly resolved and well-supported tree topologies for the phylogenomic relationships within Orchidaceae (Supplementary Material 3). Within Epidendroideae, Cymbidiinae was monophyletic and sister to all other Cymbidieae including Dipodiinae (SH-aLRT/UFboot 100/100; Figure 2). *Dipodium* was retrieved as the next diverging lineage within Cymbidieae and monophyletic with maximum support values (SH-aLRT/UFboot 100/100; Figure 2).

Within *Dipodium*, section *Leopardanthus* was placed as a sister group to section *Dipodium* with maximum support values (SH-aLRT/UFboot 100/100; Figure 3). Section *Dipodium* was resolved as monophyletic and divided into six highly supported lineages. The

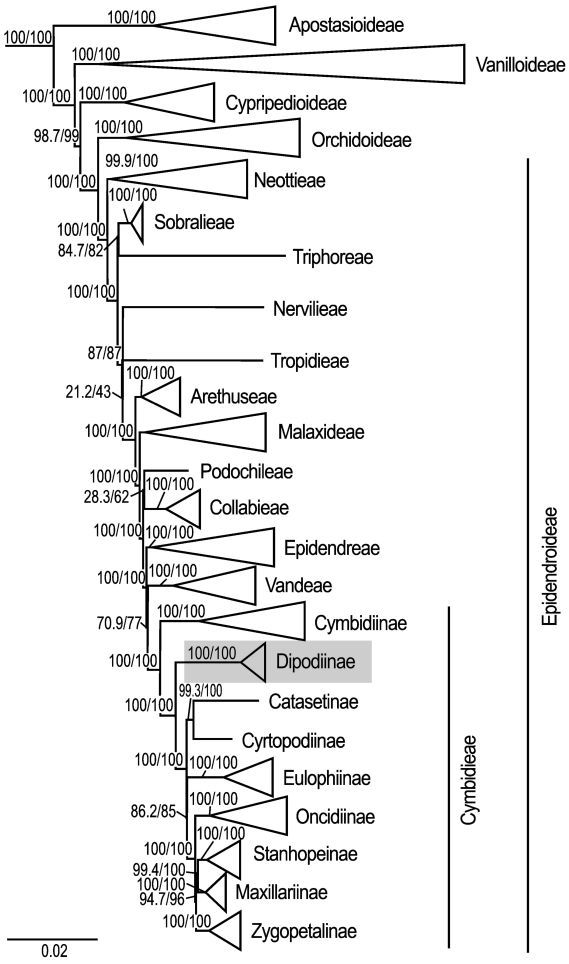

FIGURE 2
Phylogenetic relationships among major orchid lineages and placement of subtribe Dipodiinae in Cymbidieae. Maximum likelihood tree of 148 taxa based on 68 plastid loci. Support values are shown above each branch, and SHaLRT is followed by UFBoot values. Scale bar represents branch length, along which 0.02 per-site substitutions are expected. Detailed phylogeny is provided in Supplementary Material 3.

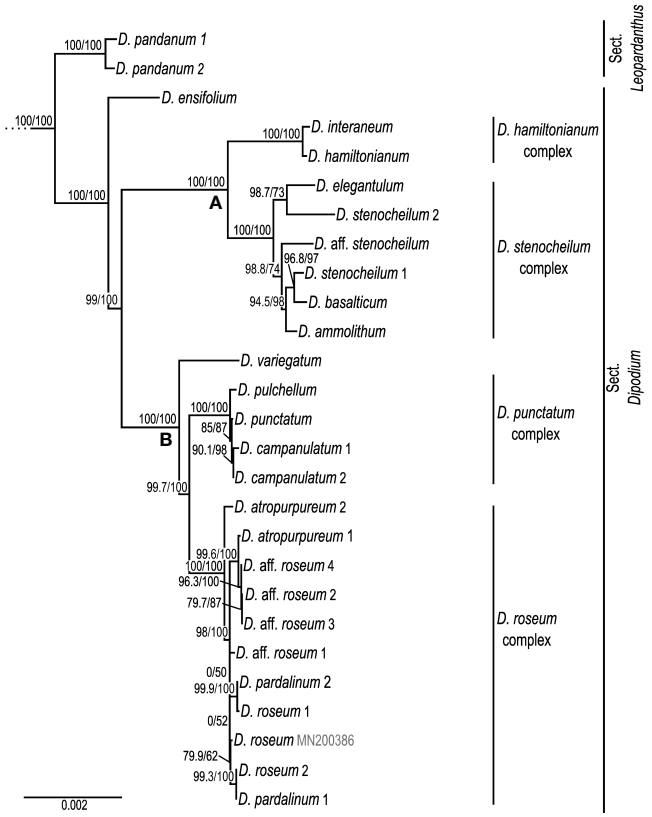

FIGURE 3
Phylogenetic relationships in *Dipodium*. Maximum likelihood tree based on 68 plastid loci and 148 taxa (outgroups not shown). Support values are given above each branch, and SHaLRT is followed by UFBoot values. Scale bar represents branch length, along which 0.002 per-site substitutions are expected. **A** and **B** refer to the two major clades in sect. *Dipodium*.

leafy species *D. ensifolium* was placed as a sister to all leafless species of the section (SH-aLRT/UFboot 100/100; Figure 3). Next, sect. *Dipodium* was split into two main clades, A and B (SH-aLRT/UFboot 99/100; Figure 3). Clade A split into two lineages, the *D. hamiltonianum* complex and the *D. stenocheilum* complex, receiving maximum nodal support (SH-aLRT/UFboot 100/100; Figure 3). The *D. hamiltonianum* complex comprised the two species, *D. hamiltonianum* and *D. interaneum*. The *D. stenocheilum* complex included *D. ammolithum*, *D. basalticum*, *D. elegantulum*, *D. stenocheilum*, and *D.* aff. *stenocheilum*. *D. stenocheilum* was retrieved as non-monophyletic (Figure 3).

Clade B resolved *D. variegatum* as a sister to the remaining species of the clade (SH-aLRT/UFboot 100/100). The remainder was split into the *D. punctatum* complex and the *D. roseum* complex (SH-aLRT/UFboot 99.7/100; Figure 3). The *D. punctatum* complex comprised three species, *D. campanulatum*, *D. pulchellum*, and *D. punctatum*. The phylogenetic divergence between these three species was shallow and supported by interspecific relationships within the complex low. The *D. roseum* complex comprised four taxa, namely, *D. atropurpureum*, *D. pardalinum*, *D. roseum*, and *D.* aff. *roseum*. Resolution and support for interspecific relationships within the *D. roseum* complex were low overall.

3.2 Divergence-time estimations

Absolute times of divergence under strict and optimised relaxed clocks for Orchidaceae based on 30 plastid loci and 134 taxa showed similar results. Strict clock models consistently yielded slightly older age estimates than the analyses based on the relaxed clock models (Supplementary Material 4). Model comparison using AICM (Fabozzi et al., 2014) identified the relaxed clock model under the birth–death speciation model as the best-fit model for the dataset (Supplementary Material 4).

The Bayesian relaxed clock tree topology and the maximum likelihood phylogeny agreed overall in major relationships within Orchidaceae and the placement of species within *Dipodium*. Epidendroideae was estimated to have emerged ca. 77.7 Ma [highest posterior density (HDP), 74.2–81.5] with the stem age of subtribe Cymbidieae placed in the Eocene, ca. 42.2 Ma (HDP, 34.3–50.1) (Supplementary Materials 4, 5). The stem age of subtribe

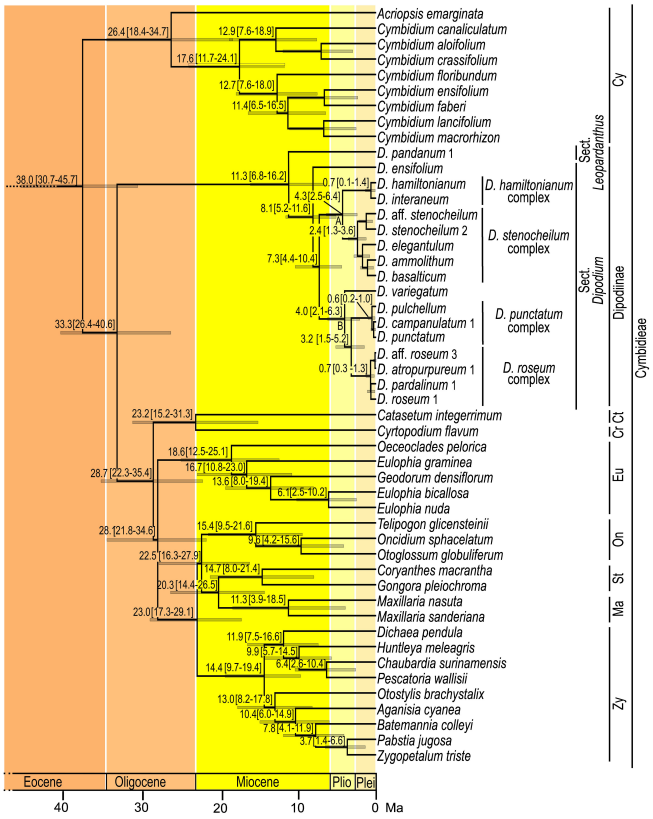

FIGURE 4
Chronogram of Cymbidieae. Maximum-clade-credibility tree from Bayesian divergence-time estimation in BEAST2 based on 30 plastid loci and an optimised lognormal molecular clock model under the birth–death prior (outgroups not shown). Divergence times (million years ago) are shown at each node, together with 95% highest posterior density (HDP) values indicated by grey bars and values in parentheses. **A** and **B** refer to the two major lineages within sect. *Dipodium*. Cy, Cymbidiinae; Ct, Catasetinae; Cr, Cyrtopodiinae; Eu, Eulophiinae; On, Oncidiinae; St, Stanhopeinae; Ma, Maxillariinae; Zy, Zygopetalinae; Plio, Pliocene; Plei, Pleistocene. Outgroups to Cymbidieae not shown. Detailed chronogram is provided in Supplementary Material 5.

Cymbidiinae, the first diverging lineage in Cymbidieae, was placed in the late Eocene, ca. 38.0 Ma (HDP, 30.7–45.7) (Figure 4). Stem diversification of Dipodiinae was estimated to have commenced ca. 33.3 Ma (HDP, 26.4–40.6) in the early Oligocene (Figure 4). Crown diversification of Dipodiinae was estimated to have commenced much later, in the late Miocene with sections *Dipodium* and *Leopardanthus* diverging ca. 11.3 Ma (HDP, 6.8–16.2) (Figure 4). The crown age of section *Dipodium* was estimated to be ca. 8.1 Ma (HDP, 5.2–11.6) in the late Miocene with the divergence of the leafy species, *D. ensifolium*, from the remainder of section *Dipodium* (Figure 4). The crown age of the remainder of the section, i.e., all leafless species, was estimated to be ca. 7.3 Ma (HDP, 4.4–10.4) (Figure 4). Within this leafless clade, two subclades, each containing two species complexes, were resolved. The crown age of the clade comprising the *D. hamiltonianum* complex and the *D. stenocheilum* complex was estimated to be ca. 4.3 Ma (HDP, 2.5–6.4) in the early Pliocene (Figure 4), which is congruent with estimations of the crown age of clade B (comprising *D. variegatum* and the two complexes *D. punctatum* and *D. roseum*) (Figure 4). The *D. stenocheilum* complex had a crown age of ca. 2.4 Ma (HDP, 1.3–3.6) in the early Pleistocene. The three remaining complexes had crown ages estimated to the mid-Pleistocene (*D. hamiltonianum* complex, ca. 0.7 Ma, HDP, 0.1–1.4; *D. punctatum complex*, ca. 0.6 Ma, HDP, 0.2–1.0, and *D. roseum* complex, ca. 0.7 Ma, HDP, 0.3–1.3) (Figure 4).

3.3 Characterisation of *Dipodium* plastomes

Complete reference-guided plastome assemblies and annotations were successfully carried out for 24 *Dipodium* samples, representing all Australian species of section *Dipodium* including two recently discovered species of section *Dipodium* (*D. ammolithum* and *D. basalticum*), two putatively new species of section *Dipodium* (*D.* aff. *roseum* and *D.* aff. *stenocheilum*), and one species of section *Leopardanthus* (*D. pandanum*) (Table 2). However, *de novo* assemblies using SPAdes and GetOrganelle often did not yield complete circular plastomes (Supplementary Material 6). Two successful complete *de novo* assemblies (the leafy *D. pandanum* 1 and the leafless *D. atropurpureum* 1) as well as partial contigs from other *de novo* assemblies were compared to the respective reference-guided assembled plastomes. In the two complete *de novo* assembled plastomes (*D. pandanum* 1 and *D.*

TABLE 2 Comparison of plastome features in *Dipodium*.

Sample	Plastome length (bp)	SSC length (bp)	IRA/B length (bp)	LSC length (bp)	GC content	Total CDS (unique CDS)	Total tRNA (unique tRNA)	Total rRNA (unique rRNA)	Total pseudogenes	Total lost genes	Total functional genes
D. pandanum 1	146,204	13,849	24,762	82,831	37.0%	74 (68)	38 (30)	8 (4)	9	3	120
D. ensifolium	150,084	16,756	25,497	82,334	36.9%	74 (68)	38 (30)	8 (4)	10	3	120
Dipodium hamiltonianum complex											
D. hamiltonianum	145,902	14,384	24,929	81,660	37.1%	74 (68)	39 (31)	8 (4)	10	3	121
D. interaneum	146,497	14,635	24,951	81,960	37.0%	74 (68)	39 (31)	8 (4)	10	3	121
Dipodium stenocheilum complex											
D. elegantulum	144,865	14,003	24,606	81,650	36.9%	74 (68)	39 (31)	8 (4)	9	4	121
D. stenocheilum 2	145,589	13,821	25,127	81,514	37.0%	74 (68)	39 (31)	8 (4)	9	4	121
D. stenocheilum 1	144,751	12,670	25,009	82,063	36.9%	74 (68)	38 (30)	8 (4)	9	4	120
D. basalticum	148,478	15,238	25,640	81,960	37.0%	74 (68)	38 (30)	8 (4)	10	3	120
D. ammolithum	147,842	14,697	25,600	81,946	37.0%	74 (68)	39 (31)	8 (4)	9	4	121
D. variegatum	142,949	12,039	24,436	82,038	37.0%	74 (68)	38 (30)	8 (4)	6	7	120
Dipodium punctatum complex											
D. pulchellum	151,425	15,735	26,369	82,952	36.9%	74 (68)	38 (30)	8 (4)	11	2	120
D. punctatum	151,181	15,737	26,136	83,172	37.0%	74 (68)	38 (30)	8 (4)	11	2	120
D. campanulatum 1	146,390	13,602	25,284	82,220	36.9%	74 (68)	37 (29)	8 (4)	12	2	119
D. campanulatum 2	149,050	14,266	25,902	82,980	37.0%	74 (68)	38 (30)	8 (4)	11	2	120
Dipodium roseum complex											
D. atropurpureum 2	149,390	15,509	25,909	82,063	36.9%	74 (68)	38 (30)	8 (4)	10	3	120
D. atropurpureum 1	150,481	15,633	26,399	82,050	36.9%	74 (68)	38 (30)	8 (4)	9	4	120
D. aff. *roseum* 4	152,282	16,426	26,630	82,596	36.9%	73 (67)	38 (30)	8 (4)	11	3	119
D. aff. *roseum* 2	150,462	15,514	26,388	82,172	36.9%	74 (68)	38 (30)	8 (4)	9	4	120
D. aff. *roseum* 3	152,956	16,571	26,817	82,751	36.9%	74 (68)	38 (30)	8 (4)	10	3	120
D. aff. *roseum* 1	151,791	16,362	26,424	82,581	36.9%	74 (68)	38 (30)	8 (4)	10	3	120
D. pardalinum 2	151,659	16,276	26,580	82,223	36.9%	74 (68)	38 (30)	8 (4)	10	3	120

(Continued)

10.3389/fpls.2024.1388537

TABLE 2 Continued

Sample	Plastome length (bp)	SSC length (bp)	IRA/B length (bp)	LSC length (bp)	GC content	Total CDS (unique CDS)	Total tRNA (unique tRNA)	Total rRNA (unique rRNA)	Total pseudogenes	Total lost genes	Total functional genes
Dipodium roseum complex											
D. pardalinum 1	148,174	15,283	25,494	81,903	36.8%	74 (68)	38 (30)	8 (4)	9	4	120
D. roseum 1	150,857	15,848	26,521	81,967	36.9%	74 (68)	38 (30)	8 (4)	9	4	120
D. roseum 2	147,730	14,192	25,819	81,900	36.8%	74 (68)	38 (30)	8 (4)	9	4	120

atropurpureum 1) and the respective reference-guided plastomes, no fundamental structural differences were detected. Minor discrepancies concerned some degraded plastid loci (mainly *ndh* genes). In these degraded plastid loci, bases tended to be recovered to a slightly greater extent in the reference-guided assemblies compared to *de novo* assemblies. These general findings agreed with the comparison of partial contigs from the *de novo* assemblies for most other samples to the respective reference-guided assembled plastomes. Plastome assemblies for *D. pandanum* 2 and *D.* aff. *stenocheilum* showed an insufficient mean coverage (<30) for non-coding regions, which caused unsolved gaps and ambiguous bases that could not be reliably resolved with the reference-guided or *de novo* assemble approaches. The number of paired-end trimmed reads for the successfully reference-guided assembled complete plastomes ranged from 332,604 (*D. pandanum* 1) to 27,999,734 (*D. pardalinum* 2), and the mean coverage ranged from 31x to 627x (Supplementary Material 6).

3.3.1 Plastome features and structural variations within *Dipodium* plastomes

Plastome sizes of *Dipodium* ranged from 142,949 bp (*D. variegatum*) to 152,956 bp (*D.* aff. *roseum* 3) (Table 2, Figure 5; Supplementary Material 7). The largest average plastome size (150,578 bp) was found in the *D. roseum* complex, closely followed by the leafy *D. ensifolium* (150,084 bp) and the *D. punctatum* complex (149,512 bp). Plastome sizes within the *D. stenocheilum* complex were markedly lower with an average size of 146,305 bp. Similarly, small plastomes were also found in *D. hamiltonianum* (145,902 bp), *D. interaneum* (146,497 bp), and the leafy climber *D. pandanum* 1 (sect. *Leopardanthus*) (146,204 bp) (Table 2). *Dipodium* plastomes possess the typical quadripartite structure of angiosperms, with the SSC region ranging from 12,039 bp (*D. variegatum*) to 16,756 bp (*D. ensifolium*), the LSC region ranging from 81,514 bp (*D. stenocheilum* 2) to 83,172 bp (*D. punctatum*), and the pair of IRs ranging from 24,436 bp (*D. variegatum*) to 26,817 bp (*D.* aff. *roseum* 3) (Table 2).

Total mean GC content of *Dipodium* plastomes was 36.9%, ranging between 36.8% (*D. roseum* 2 and *D. pardalinum* 1) and 37.1% (*D. hamiltonianum*) (Table 2). Within the *D. roseum* complex, the GC content was 36.8%–36.9%, followed by the *D. punctatum* complex (36.9%) and *D. stenocheilum* complex (37.0%), and the highest GC content was 37.1% and 37.0% (*D. hamiltonianum* and *D. interaneum*, respectively) (Table 2).

The plastid genes of each plastome were rated as functional, moderately to severely pseudogenised, or physically lost. The total number of functional genes in *Dipodium* plastomes ranged slightly from 119 to 121, including a total of 73 or 74 functional protein-coding sequence regions [protein-coding sequence (CDS)] (68 or 69 unique CDS), 37 to 39 functional tRNA genes (30 or 31 unique tRNA genes), and eight rRNA genes (four unique rRNA genes) (Table 2).

The IR region was largely conserved among all examined *Dipodium* plastomes. All species showed six duplicated coding regions in the IRs (i.e., *rpl*2, *rpl*23, *rps*7, *rps*12, *rps*19, and *ycf*2) and all four rRNA genes (Table 3). Most plastomes showed eight duplicated tRNA genes in the IR regions with the exception of the

10.3389/fpls.2024.1388537

plastomes of *D. interaneum* and *D. elegantulum*, which comprised a duplicated *trn*V-GAC within the IRB, and the plastomes of *D. ammolithum*, *D. hamiltonianum*, and *D. stenocheilum* 2, which contained a duplicated *trn*V-GAC within the IRA (Table 3, Figures 5B, C). All plastomes contained 16 functional intron genes (i.e., *atp*F, *clp*P, *pet*B, *pet*D, *rpl*2, *rpl*16, *rpo*C1, *rps*12, *rps*16, *trn*A-UGC, *trn*G-UCC, *trn*I-GAU, *trn*K-UUU, *trn*L-UAA, *trn*V-UAC, and *ycf*3), except for *D. pandanum* 1, which possessed two pseudogenes with introns (i.e., *ndh*A and *ndh*B) (Table 3, Figure 5). The *rps*12 gene was *trans*-spliced with the 5′ end located in the LSC region, and the 3′ end was duplicated in the IRs in all studied plastomes (Figure 5; Supplementary Material 7).

The SSC region was found to vary the most among the examined samples. All plastomes showed a contraction of the SSC with a reduction of 20%–40% compared to the average size of the angiosperm SSC regions (ca. 20 kb) (Ruhlman and Jansen, 2014).

Three plastomes (*D. pandanum* 1, *D. stenocheilum* 1, and *D. variegatum*) lost the *ndh*F gene. This complete loss of the *ndh*F gene resulted in the *ycf*1 fragment being located in the vicinity of the *rpl*32 (Figures 5B–D) and caused a boundary shift of the IRB/SSC region located at the 3′ end of the *ycf*1 fragment and spacer region of *rpl*32 (Figure 5). All other plastomes exhibited a severely truncated *ndh*F gene but did not exhibit an IRB/SSC boundary shift (Figure 5; Supplementary Material 7). The IRA/SSC junction

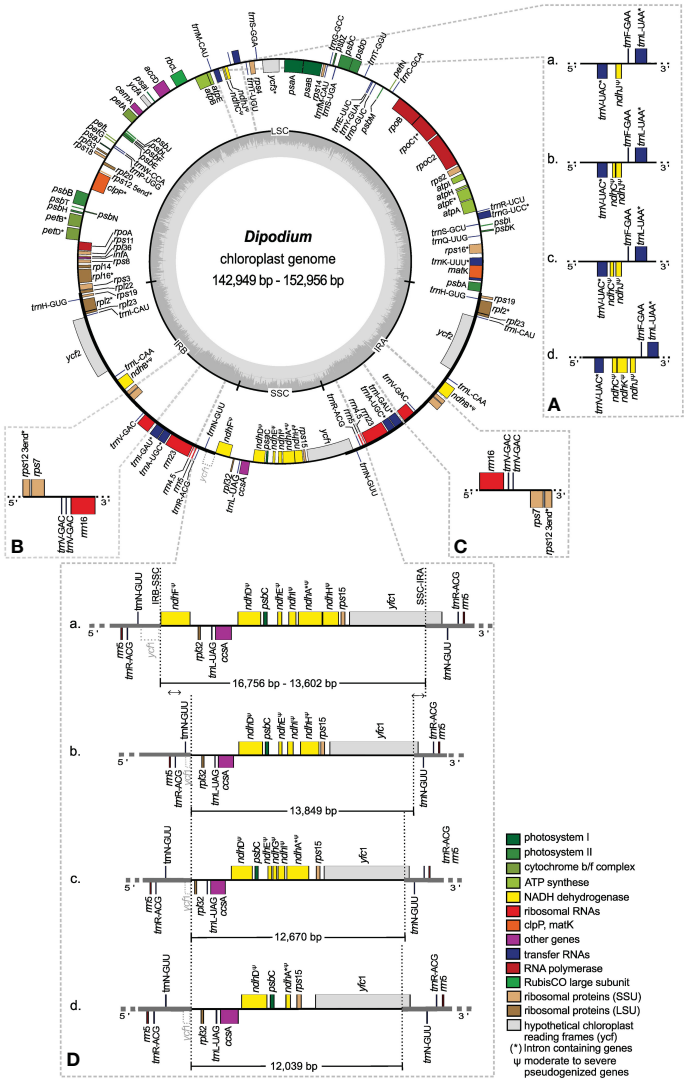

FIGURE 5
Plastome map and boundary shifts in *Dipodium*. The plastome of *D. atropurpureum* 2 is illustrated as representative and shown as a circular gene map with the smallest and the largest *Dipodium* plastome of this study. Genes outside the circle are transcribed in a clockwise direction, and those inside the circle are transcribed in a counterclockwise direction. The dark grey inner circle corresponds to the G/C content, and the lighter grey corresponds to the A/C content. The major distinct regions of complete *Dipodium* plastomes are compared in each detailed enlarged box **(A–D)**. **(A)** Note that each representative block **(A–D)** has pseudogenised or lost *ndh*J, *ndh*K, or *ndh*C gene. **(B, C)**. Duplication of *trn*V-GAC in the inverted repeat regions of *D. interaneum* (IRB), *D. hamiltonianum* (IRA), *D. elegantulum* (IRB), *D. stenocheilum* 2 (IRA), and *D. ammolithum* (IRA). **(D)** Each block **(A)** as representative *D. roseum* 2; **(B)** *D. pandanum* 1; **(C)** *D. stenocheilum* 1; **(D)** *D. variegatum*) shows differences in the length (bp) of the SSC region caused through loss or pseudogenisation of *ndhF*, *ndhD*, *ndhE*, *ndhG*, *ndhI*, *ndhA*, or *ndhH*; note the boundary shift of the IRs/SSC region caused through the loss/pseudogenisation of *ndh*F and the inclusion of the functional *ycf*1 and the *ycf1* fragment (grey, dashed line) into the IRs. SSC, small single copy; LSC, large single copy, IRA/B, inverted repeat A/B.

in all examined plastomes was located within the 5′ portion of the functional *ycf*1 gene, ranging from 97 bp (*D. pandanum* 1) to 1,072 bp (*D.* aff. *roseum* 3) (Figure 5).

In contrast to the instability of the IR/SSC boundaries, IR/LSC boundaries were found to be relatively stable. For all studied plastomes, the LSC/IRA boundaries were located near the 3′ end of *psb*A (Figure 5). Variations within the LSC regions were limited to the operon, which contained *ndh*C, *ndh*J, *ndh*K (Figure 5A), and the independent pseudogenisation of *cem*A in the plastome of *D.* aff. *roseum* 4 and *trn*D-GUC in the plastome of *D. campanulatum* (Table 3; Supplementary Material 7).

3.3.2 *ndh* gene degradation and loss in *Dipodium*

All *ndh* genes exhibited varying degrees of putative loss or pseudogenisation; not a single *ndh* gene remained functional in the examined *Dipodium* plastomes (Table 3, Figures 5, 6).

The most severe *ndh* gene loss occurred in the plastome of *D. variegatum*, with *ndh*A, *ndh*B, *ndh*D, and *ndh*K severely pseudogenised and *ndh*J moderately pseudogenised.

The greatest degradation processes within *Dipodium* occurred for the *ndh*G gene, which was putatively lost in almost all plastomes, except *D. stenocheilum* 1, which retained a severely pseudogenised *ndh*G gene (Figure 6). This was followed by *ndh*K, which was lost in 19 out of 24 plastomes (*D. ensifolium*, *D. hamiltonianum*, *D. interaneum*, the *D. roseum* complex, and the *D. stenocheilum* complex) (Figure 6). In the six remaining plastomes, *ndh*K was conserved to different degrees. *D. punctatum*, *D. pulchellum*, and *D. campanulatum* 2 retained more than 90% of the homologous bases compared to the functional *ndh*K gene of *M. coccinea* (KP205432, Kim et al., 2015) but showed severe frameshift mutations and indels, which caused several internal stop codons. The plastomes with severely pseudogenised *ndh*K genes exhibited large truncations.

Nine *Dipodium* samples (*D. ammolithum*, *D. atropurpureum* 1, *D. elegantulum*, *D. pardalinum* 1, *D. roseum* 1 and 2, *D.* aff. *roseum* 2, *D. stenocheilum* 2, and *D. variegatum*) putatively lost the *ndh*C gene. In *D. punctatum*, *ndh*C was moderately pseudogenised, and in the remaining plastomes, *ndh*C was severely pseudogenised (Figure 6). Only *D. ensifolium* showed an intact start codon for the *ndh*C gene but suffered a severe truncation with the loss of ca. 50% of homologous bases compared to the functional *ndh*C gene of *M. coccinea* (KP205432, Kim et al., 2015).

In *D. pandanum* 1, *D. stenocheilum* 1, and *D. variegatum*, the *ndh*F gene was putatively lost (Figure 6). All other samples possessed severely truncated *ndh*F genes with absent start codons and multiple internal stop codons. The *ndh*H gene was present in *D. pandanum* 1, possessing a length of 1,176 bp (99.2% of homologous length compared to *M. coccinea*; KP205432, Kim et al., 2015). In most other samples, the *ndh*H gene was degraded, possessing several stop codons. *D. stenocheilum* 1 and *D. variegatum* lost the *ndh*H gene (Figures 5, 6).

Moreover, *ndh*E, *ndh*I, and *ndh*A were found to be putatively lost in the plastome of *D. variegatum* and *D. pandanum* 1 (Figures 5, 6). No gene loss occurred for *ndh*B, *ndh*D, and *ndh*J; however, all three genes exhibited various degrees of degradation within all examined *Dipodium* plastomes and were either moderately or severely pseudogenised due to internal stop codons or frameshift mutations.

The *ndh*D gene was found to have undergone the fewest degradation processes in regard to gene length, which was largely conserved ranging from 1,122 bp (*D. campanulatum* 1) to 1,521 bp

TABLE 3 List of genes identified in the plastomes of *Dipodium*.

Gene group	Gene name
Transfer RNA genes	*trn*A-UGC*[a], *trn*C-GCA, *trn*D-GUC[d], *trn*E-UUC, *trn*F-GAA, *trnf*M-CAU, *trn*G-GCC, *trn*G-UCC*, *trn*H-GUG[a], *trn*I-CAU[a], *trn*I-GAU*[a], *trn*K-UUU*, *trn*L-CAA[a], *trn*L-UAA*, *trn*L-UAG, *trn*M-CAU, *trn*N-GUU[a], *trn*P-UGG, *trn*Q-UUG, *trn*R-ACG[a], *trn*R-UCU, *trn*S-GCU, *trn*S-GGA, *trn*S-UGA, *trn*T-GGU, *trn*T-UGU, *trn*V-GAC[ab], *trn*V-UAC*, *trn*W-CCA, *trn*Y-GUA
Small subunit of ribosome	*rps*2, *rps*3, *rps*4, *rps*7[a], *rps*8, *rps*11, *rps*12*[a], *rps*14, *rps*15, *rps*16*, *rps*18, *rps*19[a]
Large subunit of ribosome	*rpl*2*[a], *rpl*14, *rpl*16*, *rpl*20, *rpl*22, *rpl*23[a], *rpl*32, *rpl*33, *rpl*36
DNA-dependent RNA polymerase	*rpo*A, *rpo*B, *rpo*C1*, *rpo*C2
Genes for photosynthesis	
Subunits of photosynthesis I	*psa*A, *psa*B, *psa*C, *psa*I, *psa*J
Subunits of photosynthesis II	*psb*A, *psb*B, *psb*C, *psb*D, *psb*E, *psb*F, *psb*H, *psb*I, *psb*J, *psb*K, *psb*L, *psb*M, *psb*N, *psb*T, *psb*Z
Subunit of Cytochrome b6f	*pet*A, *pet*B*, *pet*D*, *pet*G, *pet*L, *pet*N
Subunit of ATP synthase	*atp*A, *atp*B, *atp*E, *atp*F*, *atp*H, *atp*I
Subunit of NADH dehydrogenase	*ndh*A*[c], *ndh*B*[ac], *ndh*C[c], *ndh*D[c], *ndh*E[c], *ndh*F[c], *ndh*G[c], *ndh*H[c], *ndh*I[c], *ndh*J[c], *ndh*K[c]
Large subunits of RubisCO	*rbc*L
Ribosomal RNA genes	*rrn*5[a], *rrn*4.5[a], *rrn*16[a], *rrn*23[a]
Other genes	
Maturase	*mat*K
Envelope membrane protein	*cem*A[e]
Subunit of acetyl-CoA carboxylase	*acc*D
C-type cytochrome synthesis gene	*css*A
Protease	*clp*P*
Translation initiation factor IF-1	*inf*A
ycf genes	*ycf*1, *ycf*2[a], *ycf*3*, *ycf*4

[a]Duplicated gene.
[b]Triplicated gene in *D. hamiltonianum, D. interaneum, D. elegantulum, D. stenocheilum* 2, and *D. ammolithum*.
[c]Pseudogene or lost.
[d]Pseudogene in *D. campanulatum* 1.
[e]Pseudogene in *D.* aff. *roseum* 4.
*Intron-containing gene.

(*D. pulchellum*), and in most plastomes, *ndh*D possessed the alternative start codon ACG (Threonine). Furthermore, almost all *Dipodium* plastomes showed the canonical AUG (Methionine) start codon for *ndh*A, *ndh*B, *ndh*E, and *ndh*I. The intron-containing *ndh*A and *ndh*B genes exhibited the strongest degradation (i.e., large deletions) within the intron regions and the downstream exon in all *Dipodium* samples. Exon1 of *ndh*B was almost complete and in-frame for most plastomes and showed only one point mutation (from A to C), which resulted in a stop codon at amino acid position 68 (after 201 bp from the beginning of the first exon in *ndh*B).

Within different *Dipodium* complexes, the patterns for putative *ndh* gene losses and severe or moderate pseudogenisations were similar for examined plastomes of *D. hamiltonianum* and *D. interaneum*. Both plastomes putatively lost *ndh*G and *ndh*K and showed severe pseudogenisations of *ndh*A, *ndh*B, *ndh*C, *ndh*F, *ndh*H, and *ndh*J and a moderately pseudogenised *ndh*E gene, but differed in the level of putative pseudogenisation of *ndh*D and *ndh*I (Figure 6).

Other similarities were found in the *D. roseum* complex, in which the *ndh*D gene was moderately pseudogenised in all samples. Almost all samples of the *D. roseum* complex, except for *D. roseum* 2, harboured moderately pseudogenised *ndh*E and *ndh*I genes.

Within the same species, only *D.* aff. *roseum* 3 and *D.* aff. *roseum* 4 showed the same pattern of *ndh* gene loss and level of degradation, which was also present in the plastome of *D. pardalinum* 2. Within the *D. stenocheilum* complex, *D. stenocheilum* 1 putatively lost *ndh*I and *ndh*F.

Across other samples, only two plastome pairs (*D. ensifolium* and *D.* aff. *roseum* 1; *D. basalticum* and *D. atropurpureum* 2) shared the same pattern of *ndh* gene loss and degradation. In comparison to all other species of examined *Dipodium* plastomes, *D. variegatum* independently lost *ndh*E and *ndh*I, and *D. pandanum* 1 lost the *ndh*A gene (Figure 6).

4 Discussion

4.1 Phylogenetic placement and infrageneric relationships of *Dipodium*

This phylogenomic study based on 68 plastid loci provided strong support for the monophyly of *Dipodium* and its phylogenetic placement as an early diverging lineage within the tribe Cymbidieae. Previous phylogenetic studies included only one or two species of *Dipodium*, which precluded assessment of the monophyly of the genus (Pridgeon et al., 2009: Górniak et al. (2010); Batista et al. (2014); Chase et al., 2015; Freudenstein and Chase (2015); Kim et al., 2020; Serna-Sánchez et al., 2021; McLay et al., 2023; Pérez-Escobar et al., 2023). Our study resolved *Dipodium* as diverging early within Cymbidieae after subtribe Cymbidiinae with strong support and thus confirmed previous molecular phylogenetic studies in support of recognition of *Dipodium* at subtribal level as Dipodiinae (Li et al., 2016; Kim et al., 2020; Serna-Sánchez et al., 2021; Pérez-Escobar et al., 2023).

This phylogenomic study presents the first molecular evidence in support of the infrageneric classification of *Dipodium* into sect. *Dipodium* and sect. *Leopardanthus* (O'Byrne, 2014, 2017; Jones, 2021), lending support to the diagnostic value of vegetative traits (i.e., the presence or absence of adventitious roots) in the infrageneric classification of *Dipodium*. Section *Leopardanthus* is characterised by leafy species, which possess adventitious roots, such as *D. pandanum*. In contrast, sect. *Dipodium* comprises species without adventitious roots and includes all leafless species, the leafy species *D. ensifolium*, and the morphologically similar *D. gracile* from Sulawesi, the latter being only known from the type (destroyed) (O'Byrne, 2017). Our phylogenomic study supported the placement of the *D. ensifolium* in sect. *Dipodium*, resolved as sister to all leafless species in the section. However, further molecular study is warranted to ascertain the monophyly of the two sections based on an expanded sampling of sect. *Leopardanthus*.

Our phylogenomic study is the first to shed light on evolutionary relationships within sect. *Dipodium*, which was found to comprise six main lineages. The phylogenomic framework now allows the assessment of useful diagnostic morphological traits to characterise main lineages within the section. For example, the yellow stem and flower colour of species of the *D. hamiltonianum* complex easily distinguishes this clade from other mycoheterotrophic orchids within sect. *Dipodium* (Figure 1; Jones, 2021). Stems of remaining mycoheterotrophic species of sect. *Dipodium* are mostly greenish to dark reddish or purplish, whereas flowers vary in colour from pale white to pinkish and then purplish (Figure 1, Jones, 2021; Barrett et al., 2022). Also, sepal and petal characters were found to differ among clades: for example, species of clade A, comprising the *D. hamiltonianum* and *D. stenocheilum* complexes, possess sepals and lateral petals that are markedly narrower compared to those of species of clade B (comprising the *D. punctatum* and *D. roseum* complex) and *D. ensifolium*, the first diverging lineage within the sect. *Dipodium* (Figures 1, 3) (Jones, 2021; Barrett et al., 2022).

Phylogenetic divergence within the two species complexes in clade B, i.e., the *D. punctatum* and the *D. roseum* complexes, was shallow overall, and thus, interspecific relationships in these two groups remained largely unclear (Figure 3). Previous morphological studies highlighted difficulties in species delimitation within the *D. punctatum* complex, in particular between *D. pulchellum* and *D. punctatum* (Jones, 2021). While *D. pulchellum* is morphologically very similar to *D. punctatum*, the two species are differentiated by the intensity of their flower colours, which are richer in *D. pulchellum* and paler in *D. punctatum* (Jones and Clements, 1987). However, a morphological study by Jones (2021) revealed that the strong floral coloration of *D. pulchellum* flowers was likely due to differences in environmental factors (i.e., soil type and rainfall regime) of growing sites, and thus, Jones (2021) proposed to synonymise *D. pulchellum* with *D. punctatum*.

Similar challenges in taxonomic delimitation based on flower colours are also evident within the *D. roseum* complex. The distribution of the more widespread species *D. roseum* largely overlaps with the distributions of *D. atropurpureum* and *D. pardalinum* (ALA, 2023). In addition to a very similar growing habit, the flowers of the three species are very similar in shape and vary only slightly in coloration: *D. roseum* has bright, rosy flowers with small darker spots; *D. atropurpureum* possesses dark pinkish-

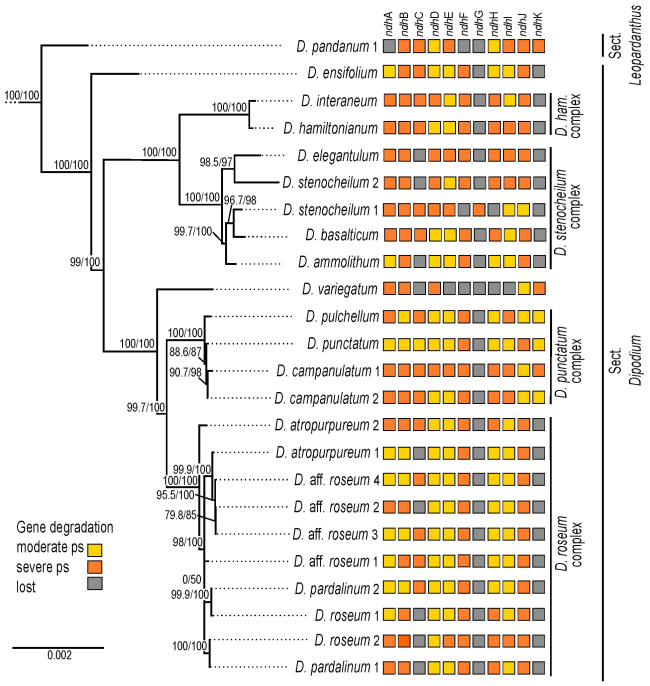

FIGURE 6
Pattern of putative *ndh* gene degradation in *Dipodium*. Gene degradation plotted against the maximum likelihood tree with focus on 24 fully assembled plastomes (outgroups not shown). Support values (SHaLRT/UFboot) are shown on each branch. ps, pseudogenisation; *D. ham.*, *Dipodium hamiltonianum*.

purple to dark reddish-purple flowers with spots and blotches; the flowers of *D. pardalinum* are pale pink to white with large reddish spots and blotches (Figure 1) (Jones, 2021). Taken together, the overlapping distribution, similar appearance, and very shallow genetic divergence found in the present study among species in the *D. roseum* complex suggest that *D. atropurpureum* and *D. pardalinum* may be colour variations of *D. roseum*. Further molecular study with more highly resolving molecular techniques such as genotyping-by-sequencing is required to rigorously assess species delimitation within *Dipodium*.

4.2 Divergence-time estimations

Our divergence-time estimations yielded results comparable to those of previous studies regarding the temporal diversification of major orchid clades (e.g., Givnish et al., 2015, 2018; Kim et al., 2020; Serna-Sánchez et al., 2021; Zhang et al., 2023). Within Epidendroideae, this study confirmed that Cymbidieae was one of the most recently diverged tribes in Orchidaceae, consistent with previous studies (e.g., Givnish et al., 2015; Serna-Sánchez et al., 2021; Zhang et al., 2023). Stem and crown diversification of Cymbidieae were estimated to have commenced at ca. 42.2 Ma and 38.0 Ma, respectively, which is similar to the estimates of Serna-Sánchez et al. (2021) and slightly younger than those of Zhang et al. (2023) (Figure 4; Supplementary Materials 4, 5).

Our study is the first to elucidate phylogenetic relationships and divergence times within *Dipodium*. Previously, only two studies included a representative of *Dipodium* (*D. roseum*, MN200368) in divergence-time estimations for Orchidaceae (Kim et al., 2020; Serna-Sánchez et al., 2021). These studies estimated the origin of *Dipodium* to be ca. 17 Ma and ca. 31 Ma. Our study placed the divergence of *Dipodium* from the other subtribes in Cymbidieae to ca. 33.3 Ma in the early Oligocene, which is closer to the findings of Serna-Sánchez et al. (2021). O'Byrne (2014) hypothesised that lineage divergence into sect. *Dipodium* and sect. *Leopardanthus* resulted from vicariance in conjunction with the break-up of Pangaea, in particular the separation of the Indian and Australian continental plates (O'Byrne, 2014). However, our divergence-time estimations show that *Dipodium* is far too young (<33 Ma) to have been influenced by the break-up of Pangaea, which occurred from the early Jurassic and onwards. Lineage divergence of sect. *Dipodium* and sect. *Leopardanthus* was estimated to be ca. 11.3 Ma in the late Miocene (Figure 4), when Australia had already assumed, approximately, its present geographical position. Rather, *Dipodium* is likely to have achieved its current distribution through range expansion between Australia and Southeast Asia across the Sunda-Sahul Convergence Zone (Joyce et al., 2021a), consistent with a general pattern of floristic exchange—the Sunda-Sahul Floristic Exchange—which was initiated as early as ca. 30 Ma (Crayn et al., 2015; Joyce et al., 2021b). However, the data are insufficient at present to resolve the ancestral area of *Dipodium* and its main lineages. Further research is needed including an increased sampling to shed light on the range evolution of *Dipodium* through ancestral range reconstruction.

Our results indicate that the Australian leafy species *D. ensifolium* diverged from the remainder of section *Dipodium* approximately 8.1 Ma (late Miocene) (Figure 4). The remainder

of the sect. *Dipodium* clade, which includes all leafless, putatively fully mycoheterotrophic species, emerged ca. 7.3 Ma (late Miocene) followed by rapid diversification from ca. 4.3 Ma onwards (early Pliocene) (Figure 4). Thus, mycoheterotrophy has most likely evolved only once within *Dipodium*, on the Australian continent during the late Miocene–early Pliocene.

From the late Miocene–early Pliocene (ca. 5 Ma), climatic conditions in Australia became increasingly arid, leading to a decline of rainforest vegetation and expansion of open sclerophyllous forests (Quilty, 1994; Gallagher et al., 2003; Martin, 2006; He and Wang, 2021). By the end of the Pliocene, Australia's landscape was similar to the present day, with much of the continent a mosaic of open woody vegetation dominated by *Eucalyptus*, *Acacia*, and Casuarinaceae (e.g., Martin, 2006). The Pleistocene (ca. 2.58–0.012 Ma) was characterised by climatic oscillations, which led to repeated forest expansion and contraction (Byrne et al., 2008). The evolution of mycoheterotrophy and the subsequent radiation of sect. *Dipodium* may have been facilitated by two factors: aridification in Australia favouring the reduction of leaf area to decrease water loss (O'Byrne, 2014) and the expansion of sclerophyll taxa and their mycorrhizal partners. Mycoheterotrophic *Dipodium* is assumed to share mycorrhizal fungi with Myrtaceae trees, especially *Eucalyptus* (Bougoure and Dearnaley, 2005; Dearnaley and Le Brocque, 2006; Jones, 2021), which explosively diversified and came to dominate most Australian forests and presumably led to increased diversity and abundance of suitable mycorrhizal partners for *Dipodium*. The rapid diversification of *Dipodium* from the Pleistocene onwards (ca. 3.2–0.3 Ma) (Figure 4) may have been driven by cycles of population fragmentation and coalescence in response to climatic oscillations.

4.3 Plastid genome evolution

4.3.1 Plastome structural features and variations

In this study, whole plastome assemblies were generated for 24 *Dipodium* samples, including representatives of all leafless, putatively full mycoheterotrophs of sect. *Dipodium* found in Australia, one leafy photosynthetic species of sect. *Dipodium* (*D. ensifolium*), and one leafy photosynthetic species of sect. *Leopardanthus* (*D. pandanum*). The overall organisation and the plastid gene content are generally conserved in most examined *Dipodium* plastomes (Figure 5, Tables 2, 3). All examined plastomes showed the typical quadripartite structure of angiosperms (Ruhlman and Jansen, 2014). However, some genomic features among several *Dipodium* plastomes were not conserved, including 1) differences in total genome length; 2) independent boundary shifts IRB/SSC/IRA within the plastome of *D. pandanum* 1, *D. stenocheilum* 1, and *D. variegatum*; 3) triplication of the *trn*V-GAC in the plastomes of *D. ammolithum*, *D. elegantulum*, *D. hamiltonianum*, *D. stenocheilum* 2, and *D. interaneum*; 4) the independent pseudogenisation of *cem*A in the plastome of *D.* aff. *roseum* 4 and *trn*D-GUC in the plastome of *D. campanulatum* 1; and 5) the pseudogenisation or loss to varying degrees of *ndh* genes (Figure 5, Table 3; Supplementary Material 7).

The total genome length of *Dipodium* plastomes displayed differences of approximately 10,000 bp between the smallest (142,949 bp; *D. variegatum*) and largest plastomes (152,956 bp, *D.* aff. *roseum* 3), which correlated with the level of *ndh* gene degradation. Some *Dipodium* plastomes were similar to the average size of orchid plastomes (152,442 bp) published on the NCBI database (286 Orchidaceae chloroplast genome, accessed on June 13, 2022; NCBI, 2022) however, most plastomes were smaller (average size *Dipodium* plastomes: 148,703 bp; Table 2). Average GC contents in *Dipodium* were very similar to the average GC content of published orchid plastomes on the NCBI database (NCBI, 2022) (ca. 36.8%; 286 Orchidaceae chloroplast genome, accessed on June 13, 2022), and all fell into the range of typical angiosperm plastomes (ca. 30%–40%) (Table 2).

4.3.2 Patterns of *ndh* gene degradation within *Dipodium*

In orchids, *ndh* gene losses and pseudogenisations, which occurred in both autotrophic and heterotrophic species, have been documented in various genera (e.g., Kim et al., 2015; Feng et al., 2016; Niu et al., 2017; Barrett et al., 2018; Roma et al., 2018; Barrett et al., 2019; Lallemand et al., 2019; Kim et al., 2020; Peng et al., 2022; Kim et al., 2023). This study is in line with these general findings in that *ndh* gene degradation was also observed within the orchid genus *Dipodium*. All chloroplast *ndh* genes in *Dipodium* plastomes exhibited varying degrees of putative pseudogenisation and loss, and not a single *ndh* gene remained functional among the examined chloroplast genomes (Table 3, Figures 5, 6). These findings include all plastomes of leafless putatively fully mycoheterotrophic species and two autotrophic leafy species (*D. pandanum* and *D. ensifolium*) and thus suggest that all examined species, independently of their nutritional status, have lost the functionality of the plastid NADH dehydrogenase complex. Hence, the last common ancestor of extant *Dipodium* is likely to have lacked a functional NDH complex. Previous studies in Cymbidiinae, the first diverging lineage in Cymbideae, found that all species studied so far exhibited at least one degraded *ndh* gene (e.g., Yang et al., 2013; Kim and Chase, 2017). As the next diverging lineage in Cymbidieae is *Dipodium*, this suggests that the degradation of *ndh* genes in Cymbidieae was likely a dynamic process from functional to non-functional. However, further research is needed, e.g., ancestral state reconstructions of gene degradation with increased taxonomic sampling. The inclusion of more species among sect. *Leopardanthus* is warranted to clarify if some *ndh* genes have remained functional in some autotrophic species of sect. *Leopardanthus*.

Previous studies examined *ndh* gene loss at the genus level and revealed an independent loss of function of the NADH dehydrogenase complex for several genera (e.g., Kim et al., 2015; Lin et al., 2015). However, comparative whole plastome studies examining gene degradation and loss among closely related mycoheterotrophic species are still scarce. For a better understanding of *ndh* gene degradation patterns, this study investigated the degree of *ndh* gene degradation among closely related orchid species (Figure 6). The greatest degradation within *Dipodium* was found for *ndh*G, which is putatively lost in almost all examined plastomes, except *D. stenocheilum* 1, which retained a putative severely pseudogenised *ndh*G (Figure 6). The *ndh*G gene is located within the SSC region.

In general, it is well established that genes in the SSC region experience higher substitution rates compared to genes located within IR regions (Ruhlman and Jansen, 2014). The latter is the case for *ndh*B, which is located in the IRs and structurally more conserved in *Dipodium* compared to most *ndh* genes located in the SSC. The greatest degree of *ndh* gene degradation occurred in *D. variegatum*, which putatively lost *ndh*C and *ndh*E–*ndh*I. All other plastomes putatively lost at least one to three *ndh* genes and showed different levels of degradation (Figure 6).

Interestingly, the level of *ndh* gene degradation varied even among closely related species within species complexes. For example, *D. stenocheilum* 1 independently lost *ndh*I and *ndh*F, whereas all other studied samples of the *D. stenocheilum* complex retained those two genes as moderately or severely pseudogenised (Figure 6). Different levels of gene degradation and loss were even found within the same species. For example, *D. atropurpureum* 1 lost *ndh*C, whereas *D. atropurpureum* 2 retained a severely pseudogenised *ndh*C (Figure 6). Moreover, the study of Kim et al. (2020) included one individual of *D. roseum*, which showed a different pattern of *ndh* gene loss and degradation to those found among the *D. roseum* samples of this study. *D. roseum* (MN200386) experienced complete loss of *ndh*A, *ndh*C–*ndh*I, and *ndh*K but retained pseudogenised *ndh*B and *ndh*J genes (Kim et al., 2020). These findings also agree with the recent comparative plastome study on *D. roseum* and *D. ensifolium*: *D. roseum* (OQ885084) has retained truncated *ndh*B, *ndh*D, and *ndh*J genes but completely lost *ndh*A, *ndh*C, *ndh*E–*ndh*I, and *ndh*K (McLay et al., 2023).

Overall, some patterns of *ndh* gene degradation found in this study in *Dipodium* are similar; however, many were unique for each individual examined. Hence, this suggests that sect. *Dipodium* has undergone a recent and active *ndh* gene degradation, which strongly implies a relaxed evolutionary selective pressure for the retention of the NDH complex.

4.3.3 IR/SSC junctions and IR instability

Orchidaceae plastomes frequently show an expansion/shift of the IR towards the SSC region (e.g., Kim et al., 2020). This instability of the IR/SSC junction is assumed to correlate with the deletion of *ndh*F and has resulted in a reduction of the SSC, as observed in several Orchidaceae plastomes (e.g., Kim et al., 2015; Niu et al., 2017; Dong et al., 2018; Roma et al., 2018) and other land plant plastomes (e.g., Amaryllidaceae, Bignoniaceae, and Orobanchaceae) (Thode and Lohmann, 2019; Könyves et al., 2021; Li et al., 2021). This study revealed reduced SSC regions for most examined plastomes, which correlated with the degradation of the *ndh* gene suite located in the SSC. Compared to typical SSC regions found in angiosperms (ca. 20 kb; Ruhlman and Jansen, 2014), the smallest SSC region was reduced by ca. 7,900 bp (*D. variegatum*), and the largest SSC region was reduced by ca. 4,700 bp (*D. ensifolium*) (Table 2, Figure 5). However, a large expansion of the IR such as found in *Vanilla* and *Paphiopedilum* plastomes (Kim et al., 2015) was not found in *Dipodium* (IR sizes ranging between 24,436 and 26,817 bp, Table 2).

In angiosperms, the *ycf*1 gene usually occupies ca. 1,000 bp in the IR (Kim et al., 2015; Sun et al., 2017). *Dipodium* plastomes in this study displayed varying positions of *ycf*1 within the IR. In plastomes in which the *ndh*F gene was completely lost or severely truncated, the portion of *ycf*1 within the IRA was mostly shorter compared to plastomes, which contained moderately truncated *ndh*F genes (Figure 5). These results are similar to the findings of Kim et al. (2015), who compared the locations of the IR/single-copy region junctions among 37 orchid plastomes and closely related taxa in Asparagales. In at least three plastomes (*D. pandanum* 1, *D. stenocheilum* 1, and *D. variegatum*), *ndh*F was independently lost, and the SSC/IRB junction was shifted into the spacer region near the *rpl*32 gene in direct adjacency to the partially duplicated *ycf*1 fragment (Figures 5B–D). These findings suggest the deletion of *ndh*F correlated with the shift of the SSC/IRB junction. Interestingly, the boundaries between SSC and IR regions were found to be variable even among closely related species, e.g., in *Cymbidium*. Some species in *Cymbidium* showed similar patterns of IR/SSC shifts (Kim and Chase, 2017) as found in *Dipodium*.

In at least five plastomes (*D. ammolithum*, *D. elegantulum*, *D. hamiltonianum*, *D. interaneum*, and *D. stenocheilum* 2), the *trn*V-GAC gene was triplicated (i.e., duplicated *trn*V-GAC version in close proximity to each other in either IRA or IRB) (Figures 5B, C, Table 3). To the best of our knowledge, similar tRNA duplication patterns within the IR regions have not yet been found in any other Orchidaceae plastomes. However, a recent study on plastomes of the angiosperm genus *Medicago* (Wu et al., 2021) yielded similar patterns. Wu et al. (2021) found three copies of the *trn*V-GAC gene in the plastomes of two closely related species within the IR (*Medicago archiducis-nicolai* and *Medicago ruthenica*), which were linked to forward and tandem repeats. Interestingly, the findings of Wu et al. (2021) support the hypothesis that repetitive sequences lead to genomic rearrangements and thus affect plastome stability. This may also apply to some *Dipodium* plastomes. However, to rule out any technical issues throughout the next-generation sequencing (NGS) process and to validate findings of duplicated tRNAs (and the above-mentioned boundaries of IR/SC regions), PCR amplification of affected regions should be carried out in future studies. However, in strong support of tRNA duplication is their independent presence within the IR of five plastomes among individuals of the same species complexes (*D. stenocheilum* complex and *D. hamiltonianum* complex). However, an increased sampling is necessary to better understand the impacts of genomic rearrangements due to repetitive sequences and thus plastome instability in *Dipodium*.

4.3.4 Evolution of mycoheterotrophy and associated plastome degradation in *Dipodium*

Heterotrophic plants are remarkable survivors, exhibiting often curious morphological, physical, or genomic modifications. Multiple heterotrophs were found to have suffered plastid genome degradations due to relaxed pressure on photosynthetic function. In recent years, evidence has accumulated that plastid genomes have undergone gene degradation in the evolutionary transition from autotrophy to heterotrophy (e.g., Wicke et al., 2016; Graham et al., 2017; Barrett et al., 2019). Among these, the first stage is the loss and pseudogenisation of genes involved in encoding the NDH complex. Interestingly, all examined plastomes of *Dipodium* have lost or

pseudogenised all 11 *ndh* genes regardless of their nutritional status (Figure 6). Two photosynthetic species with green leaves were included in this study, *D. pandanum* (sect. *Leopardanthus*) and *D. ensifolium* (sect. *Dipodium*). Degradation in *ndh* genes among photosynthetic species is not surprising and was frequently reported in previous plastome studies in land plants. The large-scale study on Orchidaceae plastomes of Kim et al. (2020) observed *ndh* gene pseudogenisation and losses among species in many epiphytes and several terrestrials that have retained their photosynthetic capacity. The NDH complex is thought to mediate the Photosystem I cyclic electron transport, fine-tune photosynthetic processes, and alleviate photooxidative stress (e.g., Yamori et al., 2015; Peltier et al., 2016; Sabater, 2021). *D. pandanum* is a terrestrial or climbing epiphytic orchid and highly localised in rainforest habitats, whereas the terrestrial *D. ensifolium* grows in open forests and woodlands (Jones, 2021); thus, both species seem to prefer shaded understory habitats. For epiphytic or terrestrial plants living in low-light habitats, it has been proposed that the NDH complex may not be essential anymore (e.g., Barrett et al., 2019). One reason for this may be that they are less exposed to photooxidative stress (e.g., Feng et al., 2016; Barrett et al., 2019). However, the NDH complex is composed of 11 chloroplast-encoded subunits and additional subunits encoded by the nucleus (e.g., Peltier et al., 2016). It has been established that genomic material was repeatedly exchanged between the nucleus, mitochondrion, and chloroplast in the evolutionary course of endosymbiosis. Thus, previous studies examined whether genes were transferred from the chloroplast to the nucleus and/or mitochondrion genome or whether nuclear genes for the NDH complex suffered under degradation. Indeed, Lin et al. (2015) reported *ndh* fragments within the mitochondrial genomes of orchids; however, no copies were found in the nuclear orchid genomes. Similar findings were reported from the orchid genus *Cymbidium* (Kim and Chase, 2017). However, further studies are needed to determine whether *ndh* gene transfer into the nucleus or mitochondrion may play a role within *Dipodium*.

The proposed subsequent next steps towards (myco-) heterotrophy is the functional loss of photosynthetic genes (e.g., *psa*, *psb*, *pet*, *rbc*L, or *rpo*) followed by genes for the chloroplast ATP synthase and genes with other functions such as housekeeping genes (e.g., *mat*K, *rpl*, and *rnn*; e.g., Graham et al., 2017; Barrett et al., 2019). Most examined *Dipodium* plastomes displayed no additional plastid gene degradation in addition to *ndh* gene degradation, except in *D.* aff. *roseum* 4, where *cem*A was pseudogenised, and in *D. campanulatum* 1, where the *trn*D-GUC gene was pseudogenised (Table 3). The *cem*A gene encodes the chloroplast envelope membrane protein and was found to be non-essential for photosynthesis; however, *cem*A-lacking mutants of the green alga *Chlamydomonas* were found to have a severely affected carbon uptake (Rolland et al., 1997) and may therefore be classified as directly involved in photosynthesis. Transfer RNA genes (*trn*) are involved in the translation process and categorised as "housekeeping" genes (e.g., Graham et al., 2017; Wicke and Naumann, 2018; Barrett et al., 2019). Moreover, similar gene degradation patterns were found in the plastomes of *D. roseum* (MN200386, Kim et al., 2020 and OQ885084, McLay et al., 2023) and *D. ensifolium* (OQ885084, McLay et al., 2023), which functionally lost all *ndh* genes. However, most photosynthesis-related genes in the plastomes of *Dipodium* were found to be functional. Thus, mycoheterotrophic species of *Dipodium* display evidence of being at the beginning of plastid gene degradation, in contrast with the majority of fully mycoheterotrophic orchids, which are in more advanced stages of degradation, e.g., *Cyrtosia septentrionalis* (Kim et al., 2019), *Epipogium* (Schelkunov et al., 2015), and *Rhizanthella* (Delannoy et al., 2011). In contrast, mycoheterotrophs such as *Corallorhiza trifida* (Barrett et al., 2018), *Cymbidium macrorhizon* (Kim et al., 2017), *Hexalectris grandiflora* (Barrett et al., 2019), and *Limodorum abortivum* (Lallemand et al., 2019) display functional losses within the plastid *ndh* genes only, and some species among them additionally lost one or two other genes, similar to findings in *Dipodium*. Interestingly, most of these species are leafless but considered putatively partially mycoheterotrophic. Suetsugu et al. (2018) demonstrated that the leafless green orchid *C. macrorhizon* contains chlorophyll and can fix significant quantities of carbon during the fruit and seed production phase and, thus, is photosynthetically active. Chlorophyll is present in *C. trifida* also, but this green, leafless coralroot is an inefficient photosynthesiser (Barrett et al., 2014). Some species among leafless orchids within sect. *Dipodium* (e.g., *D. elegantulum*, *D. stenocheilum*, and *D. variegatum*) appear green on stems (Figure 1, Jones, 2021), which suggests that they may contain some chlorophyll and be able to photosynthesise. Coupled with relatively mild plastid gene degradation compared to other fully mycoheterotrophic orchids, this suggests that some leafless species among sect. *Dipodium* may be partially mycoheterotrophic rather than fully mycoheterotrophic as has been hypothesised for *D. roseum* (Kim et al., 2020; McLay et al., 2023). However, no studies so far have examined whether leafless species among sect. *Dipodium* contain chlorophyll and whether they are capable of carrying out photosynthesis at sufficient rates. Therefore, more research is needed to assess the trophic status, including analysis of chlorophyll quantities and the ratio of photosynthetic carbon to fungal carbon for *Dipodium*.

Compared with recently published studies on mycoheterotrophic orchids such as *Corallorhiza* and *Hexalectris* (Barrett et al., 2018, 2019), which incorporated divergence-time estimations, plastomes of *Dipodium* showed the least degradation. *Hexalectris* crown age was estimated to be ca. 24 Ma, and plastomes of mycoheterotophs were more degraded compared to mycoheterotrophic plastomes of *Corallorhiza*, which diversified ca. 9 Ma onwards (Barrett et al., 2018, 2019). *Dipodium* diversified in the late Miocene ca. 11 Ma and the mycoheterotrophic lineage divergent from the autotrophic lineage ca. 8.1 Ma, which is slightly younger compared to *Corallorhiza*. Hence, time of divergence may play a role in the degree of degradation of *Dipodium* plastomes, which show an early stage of plastome degradation compared to older diverging mycoheterotrophic lineages that are in more advanced stages of plastome degradation.

5 Conclusion

This molecular phylogenomic comparative study clarified evolutionary relationships and divergence times of the genus *Dipodium* and provided support for two main lineages within *Dipodium*, corresponding to the morphologically defined sect. *Dipodium* and sect. *Leopardanthus*. A phylogenetic analysis resolved the leafy autotroph *D. ensifolium* as being part of sect. *Dipodium* and found to be in a sister group position to all leafless species in sect. *Dipodium*. Divergence-time estimations placed the divergence of the leafy species *D. ensifolium* from the remainder of section *Dipodium* in the late Miocene. Shortly after, the remaining clade including all leafless, putatively full mycoheterotrophic species within sect. *Dipodium* emerged ca. 7.3 Ma in the late Miocene followed by rapid species diversification from ca. 4.3 Ma onwards in the early Pliocene. Thus, this study indicates that mycoheterotrophy has most likely evolved only once on the Australian continent within *Dipodium* during the late Miocene and that the ancestors of putatively full mycoheterotrophic species may have had green leaves. Among the examined plastomes, all plastid *ndh* genes were pseudogenised or physically lost, regardless of the individual's nutrition strategy (i.e., autotroph versus mycoheterotroph). Thus, this study provides molecular evidence of relaxed evolutionary selective pressure on the retention of the NADH dehydrogenase complex. Mycoheterotrophic species among sect. *Dipodium* retained a full set of other functional photosynthesis-related genes and exhibited an early stage of plastid genome degradation. Hence, leafless species of sect. *Dipodium* may potentially be rather partially mycoheterotrophic than fully mycoheterotrophic.

To further disentangle evolutionary relationships in *Dipodium*, future studies based on nuclear data such as those derived from target capture sequencing and with a denser sampling at the population level are warranted. Moreover, the inclusion of a denser sampling of sect. *Leopardanthus* is warranted to clarify if some *ndh* genes may have remained functional in some of the autotrophic species of sect. *Leopardanthus*. To obtain further insights into the nutritional strategies in *Dipodium*, future studies should assess the trophic status of mycoheterotrophic species in *Dipodium* based on physiological data such as from the analysis of chlorophyll quantities and the ratio of photosynthetic carbon to fungal carbon for *Dipodium*. The Australian orchid flora harbours many more remarkable mycoheterotrophic lineages (e.g., *Danhatchia*), which offer the opportunity to further explore the evolutionary pathways to mycoheterotrophy and associated plastid genome evolution. The inclusion of autotrophic plants into comprehensive plastid phylogenetic analyses could broaden the understanding of the significance of observed *ndh* gene degradation patterns within Orchidaceae.

Data availability statement

Sequence data presented in this study are deposited in the European Nucleotide Archive repository, project number PRJEB66849, accession numbers ERR12947508 to ERR12947535 and ERR12947593 to ERR12947597 (available at: https://www.ebi.ac.uk/ena/browser/view/PRJEB66849). Processed data files were deposited in the CSIRO Data Access Portal (https://doi.org/10.25919/6wcx-0h88) under the Creative Commons Attribution-License 4.0 Creative Commons Attribution 4.0 International Licence.

Author contributions

SG: Conceptualization, Data curation, Formal analysis, Funding acquisition, Investigation, Methodology, Visualization, Writing – original draft, Writing – review & editing. MC: Conceptualization, Data curation, Funding acquisition, Investigation, Writing – review & editing. SB: Formal analysis, Investigation, Methodology, Writing – review & editing. JN: Investigation, Writing – review & editing. VP: Investigation, Writing – review & editing. DC: Funding acquisition, Writing – review & editing. PS: Investigation, Writing – review & editing. KN: Conceptualization, Data curation, Funding acquisition, Investigation, Methodology, Writing – review & editing.

Funding

The author(s) declare financial support was received for the research, authorship, and/or publication of this article. This study was supported by the Australian Biological Resources Study (Dept. of Agriculture, Water and the Environment, Australian Government NTRGP BBR210–34) and the Australian Orchid Foundation (AOF325.18; AOF357.23). SG received a research grant from the Australian Tropical Herbarium.

Acknowledgments

The authors acknowledge the contribution of Bioplatforms Australia (enabled by NCRIS) in the generation of data used in this publication. They acknowledge K. Alcock, M.D. Barrett, C. Bower, C.P. Brock, R. Crane, D.M. Crayn, W. Dowling, J. Egan, B. Gray, C. Houston, M. Jacobs, D.L. Jones, P.D. Jones, C.D. Kilgour, L. Lawler, K.R. McDonald, I. Morris, D.E. Murfet, and J. Taylor s.n. for collection of plant material used in this study. A preprint of the manuscript was released online (Goedderz et al., 2024; DOI: doi.org/10.1101/2024.02.05.578113).

Conflict of interest

The authors declare that the research was conducted in the absence of any commercial or financial relationships that could be construed as a potential conflict of interest.

Publisher's note

All claims expressed in this article are solely those of the authors and do not necessarily represent those of their affiliated organizations, or those of the publisher, the editors and the reviewers. Any product that may be evaluated in this article, or

Supplementary material

The Supplementary Material for this article can be found online at: https://www.frontiersin.org/articles/10.3389/fpls.2024.1388537/full#supplementary-material

SUPPLEMENTARY MATERIAL 1
Details of samples included in phylogenetic analysis and divergence-time estimations.

SUPPLEMENTARY MATERIAL 2
(A) Details of plastid loci included in alignment of ML-phylogenetic and divergence-time estimations. **(B)** Parsimony informative sites (Pi) for each plastid gene.

SUPPLEMENTARY MATERIAL 3
ML-Phylogenetic tree of Orchidaceae.

SUPPLEMENTARY MATERIAL 4
(A) Model comparison by AICM (Akaike Information Criterion by MCMC). **(B)** Comparison divergence-time estimations of major Orchidaceae linages (subfamilies), the tribe Cymbidieae and subtribe Dipodiinae.

SUPPLEMENTARY MATERIAL 5
Maximum-clade-credibility tree from Bayesian divergence-time estimations of Orchidaceae.

SUPPLEMENTARY MATERIAL 6
(A) Summary of reference-guided assembly features of 24 newly generated Dipodium plastomes. **(B)** Comparison of the de novo assembled contigs/plastomes using SPAdes 3.15 and GetOrganelle v1.7.7.0.

SUPPLEMENTARY MATERIAL 7
Circular plastome maps of 24 newly generated Dipodium plastomes.

References

ALA (2023) Atlas of Living (Australia). Available online at: https://www.ala.org.au (Accessed August,8 2023).

Altschul, S. F., Gish, W., Miller, W., Myers, E. W., and Lipman, D. J. (1990). Basic local alignment search tool. *J. Mol. Biol.* 215, 403–410. doi: 10.1016/S0022-2836(05)80360-2

APC. (2023). *Australian Plant Census.* (Accessed May 5, 2023).

Bankevich, A., Nurk, S., Antipov, D., Gurevich, A. A., Dvorkin, M., Kulikov, A. S., et al. (2012). SPAdes: A new genome assembly algorithm and its applications to single-cell sequencing. *J. Comput. Biol.* 19, 455–477. doi: 10.1089/cmb.2012.0021

Barrett, R. L., Barrett, M. D., and Clements, M. A. (2022). A revision of Orchidaceae from the Kimberley region of Western Australia with new species of tropical *Calochilus* and *Dipodium*. *Telopea* 25, 203–270. doi: 10.7751/telopea15711

Barrett, C. F., Freudenstein, J. V., Li, J., Mayfield-Jones, D. R., Perez, L., Pires, J. C., et al. (2014). Investigating the path of plastid genome degradation in an early-transitional clade of heterotrophic orchids, and implications for heterotrophic angiosperms. *Mol. Biol. Evol.* 31, 3095–3112. doi: 10.1093/molbev/msu252

Barrett, C. F., Sinn, B. T., and Kennedy, A. H. (2019). Unprecedented parallel photosynthetic losses in a heterotrophic orchid genus. *Mol. Biol. Evol.* 36, 1884–1901. doi: 10.1093/molbev/msz111

Barrett, C. F., Wicke, S., and Sass, C. (2018). Dense infraspecific sampling reveals rapid and independent trajectories of plastome degradation in a heterotrophic orchid complex. *New Phytol.* 218, 1192–1204. doi: 10.1111/nph.15072

Batista, J. A. N., Mota, A. C. M., Proite, K., Bianchetti, L. D. B., Romero-González, G. A., Huerta, H., et al. (2014). Molecular phylogenetics of neotropical *Cyanaeorchis* (Cymbidieae, Epidendroideae, Orchidaceae): geographical rather than morphological similarities plus a new species. *Phytotaxa* 156, 251–272. doi: 10.11646/phytotaxa.156.5.1

Bolger, A. M., Lohse, M., and Usadel, B. (2014). Trimmomatic: a flexible trimmer for Illumina sequence data. *Bioinformatics* 30, 2114–2120. doi: 10.1093/bioinformatics/btu170

Bouckaert, R., Heled, J., Suchard, M. A., Rambaut, A., and Drummond, A. J. (2014). BEAST 2: A software platform for Bayesian evolutionary analysis. *PloS Comput. Biol.* 10, 4. doi: 10.1371/journal.pcbi.1003537

Bouckaert, R., Vaughan, T. G., Barido-Sottani, J., Duchêne, S., Fourment, M., Gavryushkina, A., et al. (2019). BEAST 2.5: An advanced software platform for Bayesian evolutionary analysis. *PloS Comput. Biol.* 15, 4. doi: 10.1371/journal.pcbi.1006650

Bougoure, J. J., and Dearnaley, J. D. W. (2005). The fungal endophytes of *Dipodium variegatum* (Orchidaceae). *Australas. Mycologist* 24, 15–19.

Braukmann, T. W. A., Broe, M. B., Stefanović, S., and Freudenstein, J. V. (2017). On the brink: the highly reduced plastomes of nonphotosynthetic Ericaceae. *New Phytol.* 216, 254–266. doi: 10.1111/nph.14681

Bushnell, B. (2014). *BBMap: A fast, accurate, splice-aware aligner* (Berkeley, CA (United States: Lawrence Berkeley National Laboratory).

Byrne, M., Yeates, D. K., Joseph, L., Kearney, M., Bowler, J., Williams, M. A. J., et al. (2008). Birth of a biome: insights into the assembly and maintenance of the Australian arid zone biota. *Mol. Ecol.* 17, 4398–4417. doi: 10.1111/j.1365-294X.2008.03899.x

Chase, M. W., Cameron, K. M., Freudenstein, J. V., Pridgeon, A. M., Salazar, G., Van den Berg, C., et al. (2015). An updated classification of Orchidaceae. *Bot. J. Linn. Soc* 177, 151–174. doi: 10.1111/boj.12234

Christenhusz, M. J. M., and Byng, J. W. (2016). The number of known plants species in the world and its annual increase. *Phytotaxa* 261, 201. doi: 10.11646/phytotaxa.261.3.1

Crayn, D. M., Costion, C., and Harrington, M. G. (2015). The Sahul–Sunda floristic exchange: dated molecular phylogenies document Cenozoic intercontinental dispersal dynamics. *J. Biogeog.* 42, 11–24. doi: 10.1111/jbi.12405

Dearnaley, J. D. W., and Le Brocque, A. F. (2006). Molecular identification of the primary root fungal endophytes of *Dipodium hamiltonianum* (Orchidaceae). *Aust. J. Bot.* 54, 487. doi: 10.1071/BT05149

Delannoy, E., Fujii, S., Colas des Francs-Small, C., Brundrett, M., and Small, I. (2011). Rampant gene loss in the underground orchid *Rhizanthella gardneri* highlights evolutionary constraints on plastid genomes. *Mol. Biol. Evol.* 28, 2077–2086. doi: 10.1093/molbev/msr028

Dong, W. L., Wang, R. N., Zhang, N. Y., Fan, W. B., Fang, M. F., and Li, Z. H. (2018). Molecular evolution of chloroplast genomes of orchid species: insights into phylogenetic relationship and adaptive evolution. *Int. J. Mol. Sci.* 19, 716. doi: 10.3390/ijms19030716

Douglas, J., Zhang, R., and Bouckaert, R. (2021). Adaptive dating and fast proposals: Revisiting the phylogenetic relaxed clock model. *PloS Comput. Biol.* 17(2), e1008322. doi: 10.1371/journal.pcbi.1008322

Drummond, A. J., and Rambaut, A. (2007). BEAST: Bayesian evolutionary analysis by sampling trees. *BMC Evol. Biol.* 7, 214. doi: 10.1186/1471-2148-7-214

Fabozzi, F. J., Focardi, S. M., Rachev, S. T., and Arshanapalli, B. G. (2014). *Appendix E. Model Selection Criterion: AIC and BIC in "The basics of financial econometrics: tools, concepts, and asset management applications."* (Hoboken (New Jersey): John Wiley & Sons, Inc), 399–403.

Feng, Y. L., Wicke, S., Li, J. W., Han, Y., Lin, C. S., Li, D. Z., et al. (2016). Lineage-specific reductions of plastid genomes in an orchid tribe with partially and fully mycoheterotrophic species. *Genome Biol. Evol.* 8, 2164–2175. doi: 10.1093/gbe/evw144

Freudenstein, J. V., and Chase, M. W. (2015). Phylogenetic relationships in Epidendroideae (Orchidaceae), one of the great flowering plant radiations: progressive specialization and diversification. *Ann. Bot.* 115, 665–681. doi: 10.1093/aob/mcu253

Gallagher, S. J., Greenwood, D. R., Taylor, D., Smith, A. J., Wallace, M. W., and Holdgate, G. R. (2003). The Pliocene climatic and environmental evolution of southeastern Australia: Evidence from the marine and terrestrial realm. *Palaeogeogr. Palaeoclimatol. Palaeoecol.* 193, 349–382. doi: 10.1016/S0031-0182(03)00231-1

Gernhard, T. (2008). The conditioned reconstructed process. *J. Theor. Biol.* 253, 769–778. doi: 10.1016/j.jtbi.2008.04.005

Givnish, T. J., Spalink, D., Ames, M., Lyon, S. P., Hunter, S. J., Zuluaga, A., et al. (2015). Orchid phylogenomics and multiple drivers of their extraordinary diversification. *Proc. R. Soc B* 282, 20151553. doi: 10.1098/rspb.2015.1553

Givnish, T. J., Zuluaga, A., Spalink, D., Soto Gomez, M., Lam, V. K. Y., Saarela, J. M., et al. (2018). Monocot plastid phylogenomics, timeline, net rates of species diversification, the power of multi-gene analyses, and a functional model for the origin of monocots. *Am. J. Bot.* 105, 1888–1910. doi: 10.1002/ajb2.1178

Górniak, M., Paun, O., and Chase, M. W. (2010). Phylogenetic relationships within Orchidaceae based on a low-copy nuclear coding gene, *Xdh*: Congruence with organellar and nuclear ribosomal DNA results. *Mol. Phyl. Evol.* 56, 784–795. doi: 10.1016/j.ympev.2010.03.003

Goedderz, S., Clements, M. A., Bent, S. J., Nicholls, J. A., Patel, V. S., Crayn, D. M., et al (2024). Plastid phylogenomics reveals evolutionary relationships in the mycoheterotrophic orchid genus Dipodium and provides insights into plastid gene degeneration. *bioRxiv*. doi: 10.1101/2024.02.05.578113

Graham, S. W., Lam, V. K. Y., and Merckx, V. S. F. T. (2017). Plastomes on the edge: the evolutionary breakdown of mycoheterotroph plastid genomes. *New Phytol.* 214, 48–55. doi: 10.1111/nph.14398

Greiner, S., Lehwark, P., and Bock, R. (2019). OrganellarGenomeDRAW (OGDRAW) version 1.3.1: expanded toolkit for the graphical visualization of organellar genomes. *Nucleic Acids Res.* 47, W59–W64. doi: 10.1093/nar/gkz238

Guindon, S., Dufayard, J.-F., Lefort, V., Anisimova, M., Hordijk, W., and Gascuel, O. (2010). New algorithms and methods to estimate maximum-likelihood phylogenies: Assessing the performance of PhyML 3.0. *Syst. Biol.* 59, 307–321. doi: 10.1093/sysbio/syq010

He, Y., and Wang, H. (2021). Terrestrial material input to the northwest shelf of Australia through the Pliocene-Pleistocene period and its implications on continental climates. *Geophys. Res. Lett.* 48, e2021GL092745. doi: 10.1029/2021GL092745

Hoang, D. T., Chernomor, O., Von Haeseler, A., Minh, B. Q., and Vinh, L. S. (2018). UFBoot2: improving the ultrafast bootstrap approximation. *Mol. Biol. Evol.* 35, 518–522. doi: 10.1093/molbev/msx281

Jacquemyn, H., and Merckx, V. S. F. T. (2019). Mycorrhizal symbioses and the evolution of trophic modes in plants (R Shefferson, Ed.). *J. Ecol.* 107, 1567–1581. doi: 10.1111/1365-2745.13165

Jin, J.-J., Yu, W.-B., Yang, J.-B., Song, Y., dePamphilis, C. W., Yi, T.-S., et al. (2020). GetOrganelle: a fast and versatile toolkit for accurate *de novo* assembly of organelle genomes. *Genome Biol.* 21, 241. doi: 10.1186/s13059-020-02154-5

Jones, D. L. (2021). *A complete guide to native orchids of Australia* (Sydney: Reed New Holland Publishers).

Jones, D. L., and Clements, M. A. (1987). New orchid taxa from south-eastern Queensland. *Proc. R. Soc Queensland* 98, 128.

Joyce, E. M., Crayn, D. M., Lam, V. K. Y., Gerelle, W. K., Graham, S. W., and Nauheimer, L. (2018). Evolution of *Geosiris* (Iridaceae): historical biogeography and plastid-genome evolution in a genus of non-photosynthetic tropical rainforest herbs disjunct across the Indian Ocean. *Aust. Syst. Bot.* 31, 504–522. doi: 10.1071/SB18028

Joyce, E. M., Pannell, C. M., Rossetto, M., Yap, J. Y. S., Thiele, K. R., Wilson, P. D., et al. (2021b). Molecular phylogeography reveals two geographically and temporally separated floristic exchange tracks between Southeast Asia and Northern Australia. *J. Biogeog.* 48, 1213–1227. doi: 10.1111/jbi.14072

Joyce, E. M., Thiele, K. R., Slik, J. W. F., and Crayn, D. M. (2021a). Plants will cross the lines: climate and available land mass are the major determinants of phytogeographical patterns in the Sunda–Sahul Convergence Zone. *Biol. J. Linn. Soc* 132, 374–387. doi: 10.1093/biolinnean/blaa194

Kalyaanamoorthy, S., Minh, B. Q., Wong, T. K. F., Von Haeseler, A., and Jermiin, L. S. (2017). ModelFinder: fast model selection for accurate phylogenetic estimates. *Nat. Methods* 14, 587–589. doi: 10.1038/nmeth.4285

Katoh, K., Misawa, K., Kuma, K., Miyata, T.MAFFT (2002). A novel method for rapid multiple sequence alignment based on fast Fourier transform. *Nucleic Acids Res.* 30, 3059–3066. doi: 10.1093/nar/gkf436

Katoh, K., and Standley, D. M. (2013). MAFFT Multiple Sequence Alignment Software Version 7: Improvements in performance and usability. *Mol. Biol. Evol.* 30, 772–780. doi: 10.1093/molbev/mst010

Kim, H. T., and Chase, M. W. (2017). Independent degradation in genes of the plastid *ndh* gene family in species of the orchid genus *Cymbidium* (Orchidaceae; Epidendroideae). *PloS One* 12, e0187318. doi: 10.1371/journal.pone.0187318

Kim, Y. K., Cheon, S.-H., Hong, J.-R., and Kim, K. J. (2023). Evolutionary patterns of the chloroplast genome in vanilloid orchids (Vanilloideae, orchidaceae). *Int. J. Mol. Sci.* 24, 3808. doi: 10.3390/ijms24043808

Kim, Y. K., Jo, S., Cheon, S. H., Joo, M. J., Hong, J. R., Kwak, M. H., et al. (2019). Extensive losses of photosynthesis genes in the plastome of a mycoheterotrophic orchid, *Cyrtosia septentrionalis* (Vanilloideae: Orchidaceae). *Genome Biol. Evol.* 11, 565–571. doi: 10.1093/gbe/evz024

Kim, Y. K., Jo, S., Cheon, S. H., Joo, M. J., Hong, J. R., Kwak, M., et al. (2020). Plastome evolution and phylogeny of Orchidaceae, with 24 new sequences. *Front. Plant Sci.* 11. doi: 10.3389/fpls.2020.00022

Kim, H. T., Kim, J. S., Moore, M. J., Neubig, K. M., Williams, N. H., Whitten, W. M., et al. (2015). Seven new complete plastome sequences reveal rampant independent loss of the *ndh* gene family across orchids and associated instability of the inverted repeat/small single-copy region Boundaries (S. Aceto, Ed.). *PloS One* 10, e0142215. doi: 10.1371/journal.pone.0142215

Kim, Y. K., Kwak, M. H., Chung, M. G., Kim, H. W., Jo, S., Sohn, J. Y., et al. (2017). The complete plastome sequence of the endangered orchid *Cymbidium macrorhizon* (Orchidaceae). *Mitochondrial DNA Part B* 2, 725–727. doi: 10.1080/23802359.2017.1390411

Klimpert, N. J., Mayer, J. L. S., Sarzi, D. S., Prosdocimi, F., Pinheiro, F., and Graham, S. W. (2022). Phylogenomics and plastome evolution of a Brazilian mycoheterotrophic orchid, *Pogoniopsis schenckii*. *Am. J. Bot.* 109, 2030–2050. doi: 10.1002/ajb2.16084

Könyves, K., Bilsborrow, J., Christodoulou, M. D., Culham, A., and David, J. (2021). Comparative plastomics of Amaryllidaceae: inverted repeat expansion and the degradation of the *ndh* genes in *Strumaria truncate* Jacq. *PeerJ* 9, e12400. doi: 10.7717/peerj.12400

Lallemand, F., Logacheva, M., Le Clainche, I., Bérard, A., Zheleznaia, E., May, M., et al. (2019). Thirteen new plastid genomes from mixotrophic and autotrophic species provide insights into heterotrophy evolution in Neottieae orchids. *Genome Biol. Evol.* 11, 2457–2467. doi: 10.1093/gbe/evz170

Lam, V. K. Y., Gomez, M. S., and Graham, S. W. (2015). The highly reduced plastome of mycoheterotrophic *Sciaphila* (Triuridaceae) is colinear with its green relatives and is under strong purifying selection. *Genome Biol. Evol.* 7, 2220–2236. doi: 10.1093/gbe/evv134

Li, Z. H., Jiang, Y., Ma, X., Li, J. W., Yang, J. B., Wu, J. Y., et al. (2020). Plastid genome evolution in the subtribe Calypsoinae (Epidendroideae, Orchidaceae) (J Archibald, Ed.). *Genome Biol. Evol.* 12, 867–870. doi: 10.1093/gbe/evaa091

Li, X., Yang, J. B., Wang, H., Song, Y., Corlett, R. T., Yao, X., et al. (2021). Plastid NDH pseudogenization and gene loss in a recently derived lineage from the largest hemiparasitic plant genus *Pedicularis* (Orobanchaceae). *Plant Cell Physiol.* 62, 971–984. doi: 10.1093/pcp/pcab074

Li, M. H., Zhang, G. Q., Liu, Z. J., and Lan, S. R. (2016). Subtribal relationships in Cymbidieae (Epidendroideae, Orchidaceae) reveal a new subtribe, Dipodiinae, based on plastid and nuclear coding DNA. *Phytotaxa* 246, 37. doi: 10.11646/phytotaxa.246.1.3

Lin, C. S., Chen, J. J., Huang, Y. T., Chan, M. T., Daniell, H., Chang, W. J., et al. (2015). The location and translocation of *ndh* genes of chloroplast origin in the Orchidaceae family. *Sci. Rep.* 5, 9040. doi: 10.1038/srep09040

Logacheva, M. D., Schelkunov, M. I., and Aleksey, A. P. (2011). Sequencing and analysis of plastid genome in mycoheterotrophic orchid *Neottia nidus-avis*. *Genome Biol. Evol.* 3, 1296–1303. doi: 10.1093/gbe/evr102

Martin, H. A. (2006). Cenozoic climatic change and the development of the arid vegetation in Australia. *J. Arid Environ.* 66, 533–563. doi: 10.1016/j.jaridenv.2006.01.009

McLay, T. G. B., Bayly, M. J., Whitehead, M. R., and Fowler, R. M. (2023). Retention of an apparently functional plastome in an apparently mycoheterotrophic orchid, *Dipodium roseum* D.L.Jones & M.A.Clem. (Orchidaceae). *Aust. J. Bot.* 71, 306–317. doi: 10.1071/BT22075

Merckx, V. S. F. T. (2013). "*Mycoheterotrophy: an introduction* in *Mycoheterotrophy*," in *The Biology of Plants Living on Fungi* (Springer-Verlag, Berlin), 297–342. doi: 10.1007/978-1-4614-5209-6

Minh, B. Q., Schmidt, H. A., Chernomor, O., Schrempf, D., Woodhams, M. D., Von Haeseler, A., et al. (2020). IQ-TREE 2: New Models and efficient methods for phylogenetic inference in the genomic era. *Mol. Biol. Evol.* 37, 1530–1534. doi: 10.1093/molbev/msaa015

Nargar, K., O'Hara, K., Mertin, A., Bent, S. J., Nauheimer, L., Simpson, L., et al. (2022). Evolutionary relationships and range evolution of greenhood orchids (subtribe Pterostylidinae): Insights from plastid phylogenomics. *Front. Plant Sci.* 13. doi: 10.3389/fpls.2022.912089

NCBI (2022) National Library of Medicine. Available online at: https://www.ncbi.nlm.nih.gov (Accessed June 2, 2022).

Nguyen, L. T., Schmidt, H. A., Von Haeseler, A., and Minh, B. Q. (2015). IQ-TREE: A fast and effective stochastic algorithm for estimating maximum-likelihood phylogenies. *Mol. Biol. Evol.* 32, 268–274. doi: 10.1093/molbev/msu300

Niu, Z., Xue, Q., Zhu, S., Sun, J., Liu, W., and Ding, X. (2017). The complete plastome sequences of four orchid species: Insights into the evolution of the Orchidaceae and the utility of plastomic mutational hotspots. *Front. Plant Sci.* 8. doi: 10.3389/fpls.2017.00715

O'Byrne, P. (2014). On the evolution of *Dipodium* R. Br. *Reinwardtia* 14, 123–132. doi: 10.14203/reinwardtia.v14i1.402

O'Byrne, P. (2017). A taxonomic revision of *Dipodium* section *Leopardanthus*. *Malesian Orchid J.* 19, 5–142.

Peltier, G., Aro, E.-M., and Shikanai, T. (2016). NDH-1 and NDH-2 plastoquinone reductases in oxygenic photosynthesis. *Ann. Rev. Plant Biol.* 67, 55–80. doi: 10.1146/annurev-arplant-043014-114752

Peng, H.-W., Lian, L., Zhang, J., Erst, A. S., and Wang, W. (2022). Phylogenomics, plastome degradation and mycoheterotrophy evolution of Neottieae (Orchidaceae), with emphasis on the systematic position and Loess Plateau-Changbai Mountains disjunction of *Diplandrorchis*. *BMC Plant Biol.* 22, 5077. doi: 10.1186/s12870-022-03906-0

Pérez-Escobar, O. A., Bogarín, D., Przelomska, N. A. S., Ackerman, J. D., Balbuena, J. A., Bellot, S., et al. (2023) The origin and speciation of orchids. Available at: https://www.biorxiv.org/content/10.1101/2023.09.10.556973v3.full (Accessed January 3, 2024).

POWO (2023). Available at: http://www.plantsoftheworldonline.org/ (Accessed September 8, 2023).

Pridgeon, A. M., Cribb, P. J., Chase, M. W., and Rasmussen, F. N. (2009). *Genera Orchidacearum, Volume 5, Epidendroideae (Part 2)* (Oxford (New York: Oxford University), 585. doi: 10.1093/oso/9780198507130.001.0001

Qu, X. J., Fan, S. J., Wicke, S., and Yi, T. S. (2019). Plastome reduction in the only parasitic gymnosperm *Parasitaxus* is due to losses of photosynthesis but not housekeeping genes and apparently involves the secondary gain of a Large Inverted Repeat. *Genome Biol. Evol.* 11, 2789–2796. doi: 10.1093/gbe/evz187

Quilty, P. G. (1994). "The background: 144 million years of Australian paleoclimate and palaeogeography," in *History of the Australian vegetation: Cretaceous to recent* (Cambridge University Press, Cambridge, UK), 14–39. doi: 10.20851/Australian-vegetation

Rambaut, A., Drummond, A. J., Xie, D., Baele, G., and Suchard, M. A. (2018). Posterior summarization in Bayesian phylogenetics using Tracer 1.7. *Syst. Biol.* 67, 901–904. doi: 10.1093/sysbio/syy032

Rolland, N., Dorne, A. J., Amoroso, G., Sültemeyer, D. F., Joyard, J., and Rochaix, J. D. (1997). Disruption of the plastid *ycf*10 open reading frame affects uptake of inorganic carbon in the chloroplast of *Chlamydomonas*. *EMBO J.* 16, 6713–6726. doi: 10.1093/emboj/16.22.6713

Roma, L., Cozzolino, S., Schlüter, P. M., Scopece, G., and Cafasso, D. (2018). The complete plastid genomes of *Ophrys iricolor* and *O. sphegodes* (Orchidaceae) and comparative analyses with other orchids. *PloS One* 13, e0204174. doi: 10.1371/journal.pone.0204174

Ruhlman, T. A., and Jansen, R. K. (2014). The plastid genomes of flowering plants. 'Chloroplast Biotechnology'. *Methods Mol. Biol.* 1132, 3–38. doi: 10.1007/978–1-62703–995-6_1

Sabater, B. (2021). On the edge of dispensability, the chloroplast *ndh* genes. *Int. J. Mol. Sci.* 22, 12505. doi: 10.3390/ijms222212505

Schelkunov, M. I., Shtratnikova, V. Y., Nuraliev, M. S., Selosse, M. A., Penin, A. A., and Logacheva, M. D. (2015). Exploring the limits for reduction of plastid genomes: A case study of the mycoheterotrophic orchids *Epipogium aphyllum* and *Epipogium roseum*. *Genome Biol. Evol.* 7, 1179–1191. doi: 10.1093/gbe/evv019

Schlechter, (1911). *LII.* D. gracile *Schltr. nov. spec. in Repertorium Specierum Novarum Regni Vegetabilis* Vol. 10 (Berlin: Selbstverlag des Herausgebers), 191.

Serna-Sánchez, M. A., Pérez-Escobar, O. A., Bogarín, D., Torres-Jimenez, M. F., Alvarez-Yela, A. C., Arcila-Galvis, J. E., et al. (2021). Plastid phylogenomics resolves ambiguous relationships within the orchid family and provides a solid timeframe for biogeography and macroevolution. *Sci. Rep.* 11, 6858. doi: 10.1038/s41598–021-83664–5

Suetsugu, K., Ohta, T., and Tayasu, I. (2018). Partial mycoheterotrophy in the leafless orchid *Cymbidium macrorhizon*. *Am. J. Bot.* 105, 1595–1600. doi: 10.1002/ajb2.1142

Sun, Y., Moore, M. J., Lin, N., Adelalu, K. F., Meng, A., Jian, S., et al. (2017). Complete plastome sequencing of both living species of Circaeasteraceae (Ranunculales) reveals unusual rearrangements and the loss of the *ndh* gene family. *BMC Genom.* 9, 18(1):592. doi: 10.1186/s12864-017-3956-3

Tamura, K., Stecher, G., and Kumar, S. (2021). MEGA11: molecular volutionary genetics analysis version 11 (FU battistuzzi, ed.). *Mol. Biol. Evol.* 38, 3022–3027. doi: 10.1093/molbev/msab120

Thode, V. A., and Lohmann, L. G. (2019). Comparative chloroplast genomics at low taxonomic levels: A case study using *Amphilophium* (Bignonieae, Bignoniaceae). *Front. Plant Sci.* 10. doi: 10.3389/fpls.2019.00796

Tu, X. D., Liu, D. K., Xu, S. W., Zhou, C. Y., Gao, X. Y., Zeng, M. Y., et al. (2021). Plastid phylogenomics improves resolution of phylogenetic relationship in the *Cheirostylis* and *Goodyera* clades of Goodyerinae (Orchidoideae, Orchidaceae). *Mol. Phyl. Evol.* 164, 107269. doi: 10.1016/j.ympev.2021.107269

Wen, Y., Qin, Y., Shao, B., Li, J., Ma, C., Liu, Y., et al. (2022). The extremely reduced, diverged and reconfigured plastomes of the largest mycoheterotrophic orchid lineage. *BMC Plant Biol.* 22, 448. doi: 10.1186/s12870-022-03836-x

WFO (2023). Available online at: http://www.worldfloraonline.org (Accessed September 2023).

Wicke, S., Müller, K., De Pamphilis, C., Quandt, D., Bellot, S., and Schneeweiss, G. (2016). Mechanistic model of evolutionary rate variation en route to a nonphotosynthetic lifestyle in plants. *Proc. Nat. Acad. Sci.* 113, 9045–9050. doi: 10.1073/pnas.1607576113

Wicke, S., and Naumann, J. (2018). Molecular evolution of plastid genomes in parasitic flowering plants. *Adv. Bot. Res.* 85, 315–347. doi: 10.1016/bs.abr.2017.11.014

Wu, S., Chen, J., Li, Y., Liu, A., Li, A., Yin, M., et al. (2021). Extensive genomic rearrangements mediated by repetitive sequences in plastomes of *Medicago* and its relatives. *BMC Plant Biol.* 21, 421. doi: 10.1186/s12870-021-03202-3

Yamori, W., Shikanai, T., and Makino, A. (2015). Photosystem I cyclic electron flow *via* chloroplast NADH dehydrogenase-like complex performs a physiological role for photosynthesis at low light. *Sci. Rep.* 5, 13908. doi: 10.1038/srep13908

Yang, J. B., Tang, M., Li, H. T., Zhang, Z. R., and Li, D. Z. (2013). Complete chloroplast genome of the genus *Cymbidium*: lights into the species identification, phylogenetic implications and population genetic analyses. *BMC Evol. Biol.* 13, 84. doi: 10.1186/1471-2148-13-84

Yule, G. U. (1925). A mathematical theory of evolution, based on the conclusions of Dr. J. C. Willis, F.R.S. *Philos. Trans. R. Soc B Biol. Sci.* 213, 21–87. doi: 10.1098/rstb.1925.0002

Zhang, G., Hu, Y., Huang, M. Z., Huang, W. C., Liu, D. K., Zhang, D., et al. (2023). Comprehensive phylogenetic analyses of Orchidaceae using nuclear genes and evolutionary insights into epiphytism. *J. Integr. Plant Biol.* 65, 1204–1225. doi: 10.1111/jipb.13462

Zuckerkandl, E., and Pauling, L. (1965). Molecules as documents of evolutionary history. *J. Theor. Biol.* 8, 357–366. doi: 10.1016/0022-5193(65)90083-4